

RADIATION EFFECTS ON CONCRETE

by

Hamza K. Al-Dujaili

B.Sc., The University of Baghdad, 1962

9984

A MASTER'S THESIS

submitted in partial fulfillment of the
requirements for the degree

MASTER OF SCIENCE


Department of Nuclear Engineering

KANSAS STATE UNIVERSITY

Manhattan, Kansas

1972

Approved by:


Major Professor

**THIS BOOK
CONTAINS
NUMEROUS PAGES
THAT WERE
BOUND WITHOUT
PAGE NUMBERS.**

**THIS IS AS
RECEIVED FROM
CUSTOMER.**

**THIS BOOK
CONTAINS
NUMEROUS PAGES
WITH THE ORIGINAL
PRINTING BEING
SKEWED
DIFFERENTLY FROM
THE TOP OF THE
PAGE TO THE
BOTTOM.**

**THIS IS AS RECEIVED
FROM THE
CUSTOMER.**

LD
2668
TH
1972
A3
C.2

TABLE OF CONTENTS

1.0	INTRODUCTION	1
2.0	THEORY AND REVIEW OF LITERATURE	4
2.1	Kinetics of Thermal Decomposition of Solids	4
2.1.1	General Form of the Decomposition Curve and Descriptive Terminology	4
2.1.2	The Topochemical Nature of Solid Decomposition	7
2.2	Radiation Damage in Crystalline Solids	10
2.2.1	The Interaction between Radiation and Crystalline Solids	10
2.2.2	The Effects of Radiation on CaCO_3	11
2.2.3	Reported Effects of Radiation on the Decomposition of Crystalline Solids	12
3.0	DESCRIPTION OF EXPERIMENTAL APPARATUS	14
4.0	EXPERIMENTAL PROCEDURE	15
5.0	PRESENTATION OF DATA	23
6.0	DISCUSSION OF RESULTS AND CONCLUSIONS	32
7.0	SUGGESTIONS FOR FURTHER STUDY	45
8.0	ACKNOWLEDGEMENT	46
9.0	REFERENCES	47
10.0	APPENDICES	49
	APPENDIX A: The Calibration of the 90P3 Gas Chromatograph	50
	APPENDIX B: Power X-ray diagram	56
	APPENDIX C: Data for the Thermal Decomposition of the Powdered Calcium Carbonate and Kapitzke Concrete	68
	APPENDIX D: "Meyer Concrete"	79

LIST OF FIGURES

1. The Generalized Isothermal Decomposition Curve	5
2. CO ₂ Production Rate with time for unirradiated MnCO ₃ powder at 345°C	13
3. CO ₂ production rate with time for 9.45 Mrad pre- irradiation MnCO ₃ powder at 345°C	13
4. A view of a rubber stoppered glass vial containing the sample	17
5. A view of the glass bottle with the aluminum foil and the sample before irradiation	18
6. A view of the sealed glass bottle with aluminum foil after irradiation in the "Gammacell"	19
7. Schematic diagram of thermal decomposition system	21
8. CO ₂ production rate with time for unirradiated powdered CaCO ₃ at 1621°F	24
9. CO ₂ production rate with time for 31.2 Mrad irradiated powdered CaCO ₃ at 1621°F	25
10. CO ₂ production rate with time for 21.2 Mrad irradiated powdered CaCO ₃ at 1621°F	26
11. CO ₂ production rate with time for 16.03 Mrad Irradiated powdered CaCO ₃ at 1621°F	27
12. CO ₂ production rate with time for unirradiated powdered Kapitzke concrete at 1621°F	28
13. CO ₂ production rate with time for 12.2 Mrad and $54.95 \times 10^{16} \frac{n}{cm^2}$ irradiated powdered Kapitzke concrete at 1621°F	29

LIST OF FIGURES (continued)

14.	CO ₂ production rate with time for 19.9 Mrad irradiated powdered Kapitzke concrete at 1621°F	30
15.	CO ₂ production rate with time for 24.7 Mrad and $11.1 \times 10^{18} \frac{n}{cm^2}$ irradiated powdered Kapitzke concrete at 1621°F	31
16.	A view of the heated powdered calcium carbonate	34
17.	The effect on the total carbon dioxide production of powdered CaCO ₃ of gamma irradiation prior to thermal decomposition	36
18.	The effect on the total carbon dioxide production of powdered Kapitzke concrete of gamma irradiation prior to thermal decomposition	37
19.	Thermal decomposition curve for vibration packed CaCO ₃ powder at 1621°F. Broken line indicates the actual value	41
20.	Thermal decomposition curve for vibration packed Kapitzke concrete at 1621°F. Broken line indicates the actual value	42
1A.	Helium and carbon dioxide calibration curves for RGI F1100 Flowmeter	51
2A.	Schematic diagram of tubing arrangement	52
3A.	Calibration curve of helium mixtures with 0.0 - 0.11 mole fraction CO ₂ for 90P3 gas chromatograph	53
1B.	Arrangement for taking powder photographs. The angle RSX is 2θ, where θ is the angle of incidence on a set of crystal planes	57

LIST OF TABLES

1.	Operating Conditions for the Column and Detector in 90P3 Gas Chromatograph	20
2.	Operating Conditions for Carrier gas, filament, and Attenuator in 90P3 Gas Chromatograph	22
1-A.	Data for the Calibration of the 90P3 Chromatograph for Carbon Dioxide	55
1-C.	CO ₂ Production Rate with Time for Unirradiated CaCO ₃ at 1621°F	68
2-C.	CO ₂ Production Rate with Time for Irradiated CaCO ₃ at 1621°F	69
3-C.	CO ₂ Production Rate with Time for Irradiated CaCO ₃ at 1621°F	70
4-C.	CO ₂ Production Rate with Time for Irradiated CaCO ₃ at 1621°F	71
5-C.	CO ₂ Production Rate with Time for Unirradiated Kapitzke Concrete at 1621°F	72
6-C.	CO ₂ Production Rate with Time for Irradiated Kapitzke Concrete at 1621°F	73
7-C.	CO ₂ Production Rate with Time for Irradiated Kapitzke Concrete at 1621°F	74
8-C.	CO ₂ Production Rate with Time for Irradiated Kapitzke Concrete at 1621°F	75
9-C.	Values of α Calculated by Two Methods for CaCO ₃	76
10-C.	Values of α Calculated by Two Methods for Kapitzke Concrete	77

LIST OF TABLES (continued)

11-C.	CO ₂ Production Rate with Time for Irradiated Kapitzke Concrete at 1621°F	78
1-D.	Constituents of Kapitzke Concrete in Atomic Density Units	79
2-D.	Chemical Analysis of "Meyer Concrete"	79

NOMENCLATURE

A	The fraction of weight which is CO_2 (0.44 for CaCO_3 and 0.1324 for Kapitzke concrete)
AI, AII	Constants represent the ratio between the weight lost during thermal decomposition and the weight of dried solid (dimensionless)
C_i	Weight of carbon dioxide released (g) in each time period (2,4,6,8...)
K	The fraction of sample weight which is CO_2 (0.44 for CaCO_3 and 0.2161 for Kapitzke concrete)
M	Molecular weight of carbon dioxide (44 g/mole)
N_o	The density of germ nuclei (nuclei/cm ³)
P	Atmospheric pressure (1 atm)
R	Gas constant (82 ml·atm/mole·K°)
$R_{(24)}$	Reference 24
$R_{(25)}$	Reference 25
T	Absolute temperature (°K)
V_i	Volume of carbon dioxide released (ml) in each time period (2,4,6,8...)
W_o	Initial weight of the solid sample (g)
W_l	Weight lost during thermal decomposition (g)
W_s	Weight of dried solid (g)
W	Weight of the solid sample (g) after time t
a	A constant (dimensionless)
d_{hkl}	The interplanar spacing distance
g	Gram
(hkl)	The Miller indices
i	Time intervals (2,4,6,8,10,...)
k_o	A constant velocity of propagation (cm/sec)

k, k''	The rate constant for nucleus formation (seconds ⁻¹)
ml	Milliliter
n	The integer number (1,2,3,...etc.)
t	Time from start of thermal decomposition (seconds)
α	The cumulative value of fractional decomposition
α_i	Fractional decomposition of solid in time i (dimensionless)
θ	An angle of incidence
λ	X-ray wave length

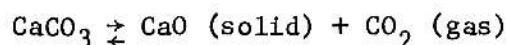
1.0 INTRODUCTION

The U.S. Atomic Energy Commission reported on October 25, 1966 that on February 16, 1966, damage to one of the eight-inch beam tubes of the 1 MW Puerto Rico Nuclear Center Research Reactor had occurred. This was due to a high pressure release in the tube which was made of solid barytes concrete completely enclosed in a 1/4" thick aluminum can. According to the AEC report (16), the cause of the pressure build-up was not known. Possible causes envisioned by the writer include either a gas producing concrete reaction or radiation induced decomposition of the concrete also producing gaseous products. Another incident also occurred (17). In this incident, a radiation shield plug ruptured within an 8" beam tube at a 1-MW pool type reactor facility. The "explosion" caused one end plate on the plug, as well as the welded-end disc on the beam tube, to be driven against the reactor; the core, however, was not damaged. The shield plug was again constructed of baryt concrete hermetically sealed within a 1/4"-thick aluminum jacket. Although the cause of this incident has not been established conclusively, suspected causes again include:

- a. Gas formation accompanying aluminum corrosion by the concrete
- b. Radiation-induced decomposition of water to produce gaseous hydrogen and oxygen.

Concrete is, of course, a basic construction material in nuclear reactor shielding. Carbonate compounds constitute some of the important components of this important material. Heat and radiation may decompose the carbonate, generating carbon dioxide, which could cause disruption and other degradation of the concrete used in nuclear reactor or other types of radiation shielding.

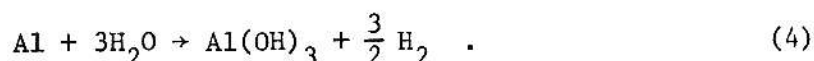
This research is concerned in part with a study of the non-equilibrium reaction kinetics of the thermal decomposition of irradiated and non-irradiated kapitzke concrete (1) and calcium carbonate in an inert atmosphere of helium gas. The dynamic reaction was followed by measuring the concentration of carbon dioxide released according to the following relation



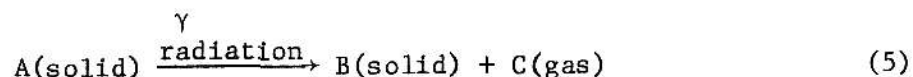
This research is also concerned with a study of the evolution of hydrogen gas due to the reaction of Kapitzke concrete with aluminum in the presence of water. Hydrogen gas is evolved according to the following relations



or in summary



Effects of gamma radiation on the kinetics of thermal decomposition have previously been studied at KSU for manganese carbonate and zinc carbonate (2) based on the relation:



where B is insoluble in A. There are available several different methods of analyzing carbon dioxide released in the above decomposition reaction. Thermogravimetric analysis and measurement of carbon dioxide pressure have been used to study equilibrium and non-equilibrium reaction kinetics for

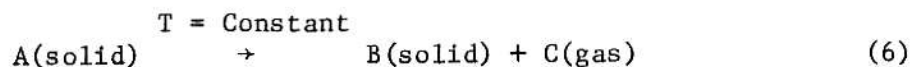
irradiated or nonirradiated carbonates (2). Gas chromatography can also be used for analysis of carbon dioxide released during decomposition. This latter procedure is comparatively fast and easily applied; therefore gas chromatographic techniques were used in this research.

2.0 THEORY AND REVIEW OF LITERATURE

2.1 Kinetics of Thermal Decomposition of Solids

2.1.1 General Form of the Decomposition Curve and Descriptive Terminology

The decomposition of solid carbonate compounds can be represented by the isothermal reaction



The decomposition can be described in terms of the fractional decomposition (α) or equivalent quantities ($\frac{d\alpha}{dt}$, ..., etc.) as a function of time. A typical decomposition can be described as follows (see decomposition curve, α vs. t , Fig. 1 as presented by Young (2)).

The A portion of Fig. 1 represents an initial rapid evolution of gas. This feature is limited to 0.1-5.0 per cent of the total decomposition. The curve is first order and the activation energy is generally about 3-5 kcal mole⁻¹.

The B portion of Fig. 1 represents the induction period. This region is characterized by a slow evolution of gas. The curve is approximately first order decay with an activation energy of about 31 Kcal mole⁻¹.

The C portion of Fig. 1 represents an acceleration period. This portion normally extends up to fractional decomposition (α_i) between 10.0-50.0 per cent of the total thermal decomposition, though α_i -values above this range are possible. The analysis of this portion yields the most significant information concerning the decomposition of the solid. It is customary to fit expressions of the form

$$\alpha = f(\exp kt) \quad (7)$$

or

$$\alpha = f(kt^n) \quad (8)$$

**THIS BOOK
CONTAINS
NUMEROUS PAGES
WITH DIAGRAMS
THAT ARE CROOKED
COMPARED TO THE
REST OF THE
INFORMATION ON
THE PAGE.**

**THIS IS AS
RECEIVED FROM
CUSTOMER.**

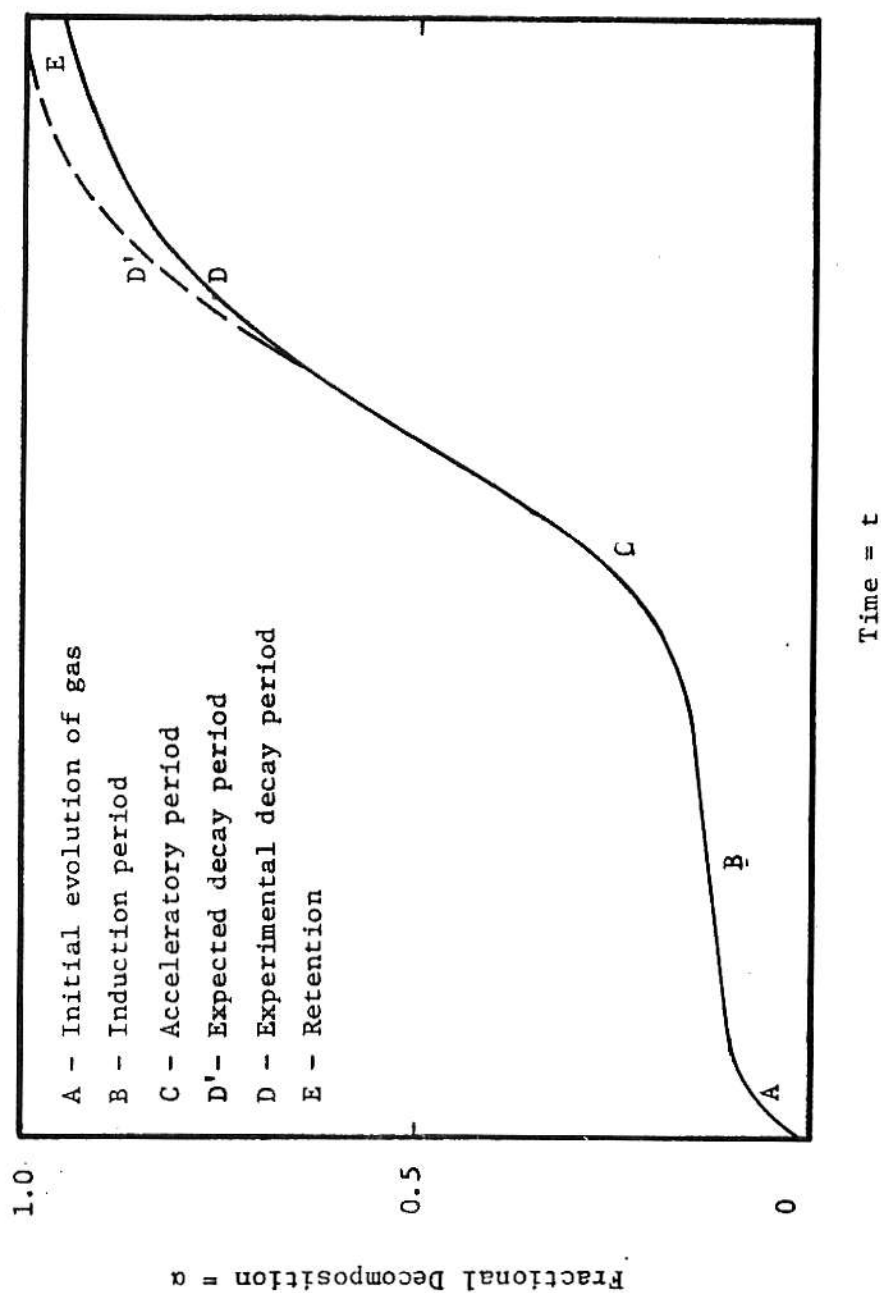


Fig. 1. The generalized isothermal decomposition curve.

to the acceleratory period. Good fits to experimental data have been obtained with these simple expressions, but in some cases it is necessary to compromise and to introduce (t_0) as an additional adjustable parameter, such that

$$\alpha = f(t - t_0)^n \quad (9)$$

The D portion of Fig. 1 represents the decay period. This portion is both more difficult to analyze satisfactorily and less valuable for interpretation of the decomposition kinetics. It depends markedly on the details of the particle size distribution present at this stage of the decomposition. However, if particle size effects can be eliminated, Section D can normally be analyzed according to a power function relation (3), e.g.,

$$\alpha = 1 - \exp(-k'' N_0 t^3) \quad (10)$$

the transition region between sections C and D defines the maximum rate of the decomposition and contains the inflection point (α_1, t_1) .

The dotted portion D' in Fig. 1 represents the actual value of D. In particular, for values of α greater than 0.98 the experimental curve is frequently observed to fall significantly below the values D'. This deviation, lettered E in Fig. 1, is termed the retention. It is evaluated by assuming the analytical function applicable throughout the major portion of D is valid up to $\alpha = 1$.

The common phenomenon of a lack of reproducibility of the decay period at high degrees of decomposition arises from a combination of particle-size effects, a reduction of chemical reactivity by poisoning or sintering, or a chemisorption of product gas on the solid product.

2.1.2 The Topochemical Nature of Solid Decomposition

In the past the analysis of decomposition curves, particularly in the acceleratory period, has been based chiefly on geometrical principles rather than on mathematical analysis. This approach was mainly due to the work of Langmuir (4) on the dissociation of calcium carbonate into two solid phases, CaO and CaCO_3 . In order that CaCO_3 may dissociate and form a separate CaO phase rather than a solid solution, the reaction must occur only at the boundary between the two phases.

In subsequent studies on decomposition, Hinshelwood and Bowen (5) discovered that the activation energy cannot be calculated directly from the temperature coefficient of the reaction without correction for variations in the extent of the reaction interface. This surface should not necessarily be identical with the external surface of the crystal. They further showed that with ammonium dichromate light crushing of partly decomposed material exposed fracture planes covered with reaction product; whereas on further grinding the interior regions of the particles were left unchanged. An observed increase in the initial reaction rate on grinding was found to be larger than that, which could be explained by the increase in the surface area alone; thus indicating the creation of "internal surfaces."

MacDonald and Hinshelwood (3) applied the new concept of reaction nuclei to solid decomposition. They adduced indirect evidence for the formation and growth of autocatalytically active nuclei with silver oxalate. They argued that the autocatalysis required to account for the acceleration in the thermal decomposition of silver oxalate for the acceleratory period could be due to either an increase in the surface area of the solid or to

the presence of nuclei of the product silver. Since this acceleration was not eliminated by grinding the silver oxalate, they concluded correctly that nuclei were formed and grew. They also showed that nucleation occurred on the external surfaces.

Roginskii and Shultz's work (3) also supported the theory of nucleus formation and growth for decomposition of potassium permanganate. Evidence of the existence of nuclei was further provided by the work of Kohlschütter (3) and Garner (7). According to their development, it was clear that the concepts of nucleus formation and growth by interfacial mechanism could account for the kinetics of the acceleratory period.

According to the topochemical model (3), the decomposition of solids is initiated by formation and growth of nuclei. These nuclei are formed on the crystal surface and grow at constant radial rates above a critical dimension. The rate of nucleation may be zero, constant, proportional to time or to $(\text{time})^2$, providing a range of power law expressions.

The concept that the reaction interface advances at a constant rate has been confirmed in the majority of cases, but there do exist important deviations from this ideal behavior. Trapping probabilities and possibility for escape of the gaseous product are major influences on the locus of nucleation in solid decompositions. One of these deviations, which arises from impedance to the release of the gaseous reaction product by layers of solid product, has been accounted for by Topley and his co-workers (8). Another deviation from the constancy of interfacial advance was found with the growth of small nuclei by Bright and Garner (3). In their study, small nuclei appear to grow more slowly than large nuclei. On the other hand, Cooper and Garner (9) have shown that small nuclei grow more rapidly than large nuclei. There

is a certain amount of evidence that this difference arises from minor and different to distinguish changes in the interfacial conditions.

The important mathematical development of the topochemical model was given by Mapel (3). In his treatment, nucleation and growth in systems consisting of spherical micro crystals was considered. Each spherical particle was divided into concentric shells. The problems of overlapping and ingestion of germ nuclei were treated by using probability considerations. Integration over all shells gave the fractional decomposition, $\alpha(t)$. Mapel's expressions for the fractional decomposition were of an integral type. However, numerical computer integration techniques are commonly available today for rigorous solutions. With a few simplifying assumptions, Mapel's expressions can be reduced to arrive at more usable simplified expressions. These simplified forms (2) are as follows:

- (1) For particle radius $r = 1$ and small values of (t) the fractional decomposition is proportional to (t^4) , therefore

$$\alpha = a t^4 \quad (11)$$

where a is a constant.

- (2) For large particle radius (r) , there is time for the surface to become completely nucleated before marked penetration occurs. Thus a contracting sphere geometry is rapidly attained and the decomposition conforms to the equation

$$\alpha = 1 - \left(1 - \frac{k_o t}{r}\right)^3 \quad (12)$$

where k_o is a constant velocity of propagation cm/sec.

- (3) For small particle radius (r), the decomposition is governed by the equation

$$\ln (1 - \alpha) = a - kt \quad (13)$$

where a is a constant.

2.2 Radiation Damage in Crystalline Solids

2.2.1 The Interaction between Radiation and Crystalline Solids

The interaction of energetic radiation with matter can be classified according to primary and secondary effects (2). The primary or direct effects include the displacement of electrons (ionization), atoms from lattice sites, excitation of both atoms and electrons without displacement, and the transmutation of nuclei. Primary effects can be produced by irradiation with energetic charged particles producing both primary atomic displacement and ionization. Irradiation with gamma-rays produces only ionization as a primary effect and atomic displacements only to a negligible extent. Irradiation with neutrons produces ionization only as a secondary process, the primary process being atomic displacement. The secondary effects are due to further excitation and disruption of lattice structure by electrons or displaced atoms produced as a primary effect. However, the most important effect of gamma-rays in solids is the ionization phenomenon.

The interaction of gamma-rays with matter occurs primarily by means of three mechanisms, the photoelectric effect, Compton scattering, and pair production. These three processes are necessary to give an accurate description of the absorption and scattering of gamma-rays in matter. The energy ranges of gamma-rays for the three processes are respectively 0.1 MeV, 0.1 to 10 MeV, and greater than 1.02 MeV. The atomic cross section for each process at a given energy depends on the atomic number, Z , of the absorber.

For reactor gamma-rays, ^{60}Co gamma-rays, and fission product sources, the Compton effect has the predominant cross section, except for absorbers of very high atomic number.

In general, radiation causes different types of defects in solids. These defect types may be summarized as follows (10):

- (a) Vacancies: This defect may result from displacements caused by collisions of energetic particles with the atoms in a solid lattice.
- (b) Interstitial atoms: Atoms displaced from their lattice sites may stop in interstitial locations.
- (c) Ionization effects: Charged particles passing through a solid may cause extensive ionization and electronic excitation leading to bond rupture.

2.2.2 The Effects of Radiation on CaCO_3

The passage of gamma rays through calcium carbonate (ionic crystal) may cause extensive ionization and electronic excitation leading to bond rupture (11). It may be postulated that CO_2 evolution and CaO formation results from the reactions



Neutron irradiation may cause lattice damage through atomic displacement. These displaced atoms are energetic charged particles and can cause electronic excitation and ionization, leading to bond rupture.

2.2.3 Reported Effects of Radiation on the Decomposition of Crystalline Solids

As noted in the previous section, nuclear radiation can induce decomposition of crystalline solids by creating crystalline defects and the breakage of chemical bonds in crystalline solids. Allen and Ghormley (12) have shown that barium nitrate decomposes when exposed to ionizing radiation, yielding nitrate ion and oxygen upon dissolution in water. Henning, Lees, and Matteson (13) have shown that sodium nitrate, potassium nitrate, and potassium chlorate exhibit decomposition when subjected to irradiation from 2-4 weeks in Argonne's heavy-water reactor. In this case decomposition results from electronic ionization and excitation rather than from the displacement of atoms by elastic collision.

Labelle (2) studied the decomposition of powdered magnesium and zinc carbonate before and after pre-irradiation with gamma radiation. The irradiated carbonates exhibited an increase in carbon dioxide production rate during the first ten minutes of their decomposition over unirradiated carbonates. Figures 2-3 show CO_2 production rates at 345 °C as a function of time for unirradiated MnCO_3 powder and for 9.45 Mrad pre-irradiated MnCO_3 powder.

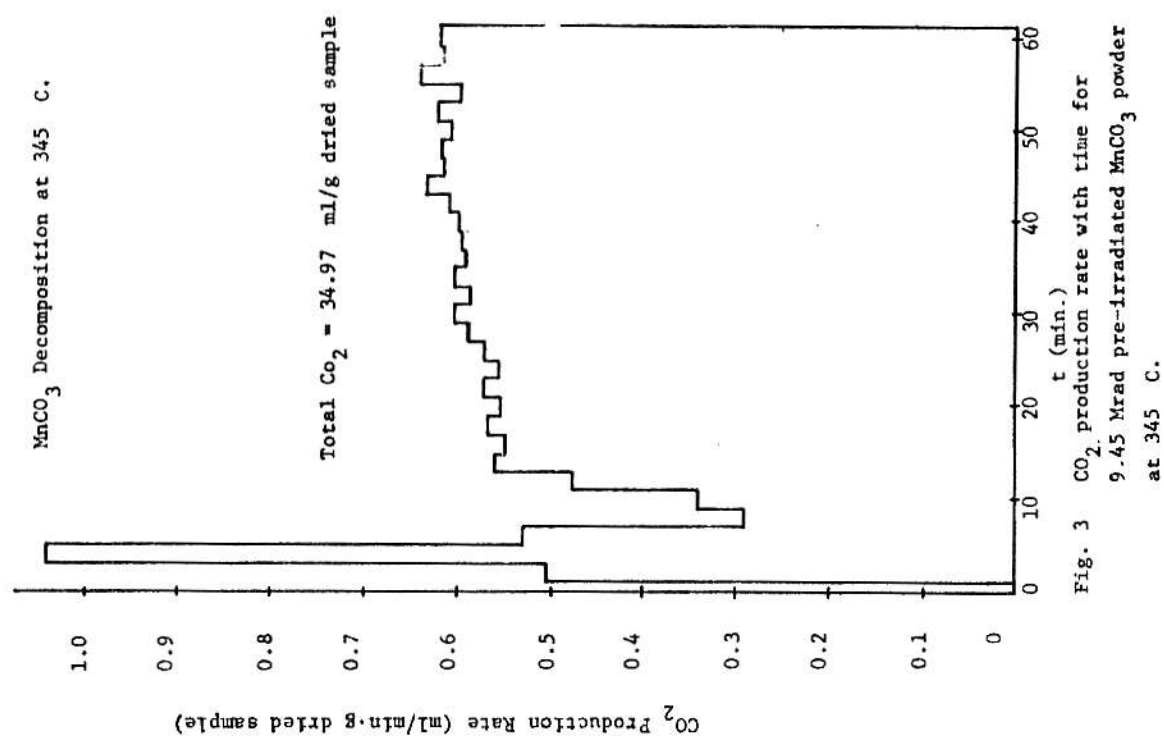


Fig. 3 CO₂ production rate with time for
9.45 Mrad pre-irradiated MnCO₃ powder
at 345 C.

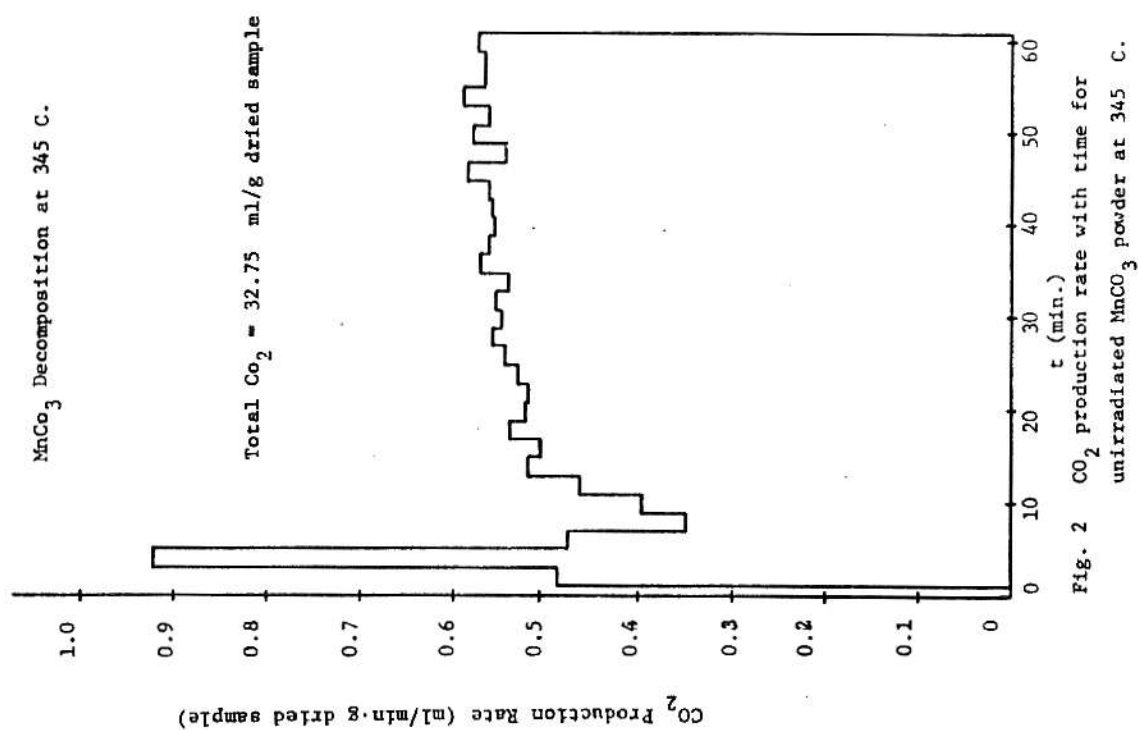


Fig. 2 CO₂ production rate with time for
unirradiated MnCO₃ powder at 345 C.

3.0 DESCRIPTION OF EXPERIMENTAL APPARATUS

A gamma irradiator, a high temperature furnace, and a gas chromatography system were used in this research. This equipment is described below.

3.1 The Gamma Irradiator

A "Gammacell" -- 220 designed by Atomic Energy of Canada, Ltd., and loaded with a 3,963 curies of ^{60}Co source on March 15, 1965, was used to irradiate the samples during this research. Inside the cell, the source is in the form of a hollow circular cylinder located inside a thick walled shield. The irradiation chamber (inside dimensions are 6 inches in diameter by 8 inches in length) is located on a movable cylinder that can be elevated for insertion or removal of a sample and lowered for irradiation of the sample within the circular cylindrical source of ^{60}Co . The irradiation chamber can be actuated by an electric timer permitting sample irradiation for a preset time in seconds, minutes or hours.

3.2 The High Temperature Furnace

A LECO (Laboratory Equipment Corporation) model 540 resistance furnace was also used. The model 540 contains two combustion tube furnaces with four silicon carbide heating elements, two of which are above the combustion tubes and two below. The furnace incorporates coarse and fine heat controls to maintain the proper level of power to the heating elements. A maximum temperature of 3000 °F can be maintained with this furnace. To detect and control furnace temperature, a platinum-rhodium thermocouple was used. For this research, the thermocouple was connected to a Barber Coleman 292 PF Capacitrol on-off type temperature controller. This controller automatically maintained the furnace temperature within ± 10 °F of the set point at 1621 °F.

3.3 The Gas Chromatography System

A Varian Aerograph Model 90-P3 Gas Chromatograph with associated strip-chart recorder, Model 30 was used to produce a quantitative analysis and record of the gas yields during thermal decomposition of CaCO_3 as well as the Kapitzke concrete.

The Model 90-P3 gas chromatograph includes the detector (thermal conductivity, four-filament, tungsten type), adsorption column temperature control oven and various other gas flow and temperature controls. The chromatographic column, a 40 foot length of 1/4 inch diameter copper tubing was packed with 60/80 mesh silica gel.

The chromatograph thermal conductivity detector indicates and measures the amount of separated components in the carrier gas due to the difference in thermal conductivity of the various gases. The detector is adjusted to zero when pure carrier gas, helium is present. Carrier gas flow rate in the work was adjusted to 50 ml/min.

The detector was designed for use with a strip chart recorder to obtain a permanent record of the results. The recorder was restricted to 1 mV full scale; however the amplitude of the output signal to the recorder was controlled by an attenuator permitting attenuation of the detector voltage by factors from 2 to 512.

4.0 EXPERIMENTAL PROCEDURE

The experimental procedure consisted of packing a carbonate sample in a stainless steel "boat" particularly designed for this work, drying the sample in a furnace to a standard condition and finally irradiating the sample using the gamma irradiator and/or KSU TRIGA Mark II Reactor. A sample was then decomposed in the high temperature furnace. A quantitative analysis of carbon dioxide content was carried out using a gas chromatograph system.

In these experiments calcium carbonate and Kapitzke (1) concrete (in powder form) were used. The powder samples were passed through a 200 mesh screen to remove any coarse particles and after preliminary drying were stored in tightly stoppered bottles.

Stainless steel "boats" (2.25 inches in length, 3/8 inch width) were used to hold the samples during irradiation and decomposition. The stainless steel "boat" was packed with the sample by a vibrational technique until it was filled to an approximately constant weight for each sample type.

Next the sample was final dried, for 24 hours using a furnace operating at 220 °F, to remove adsorbed moisture. After final drying, the sample was again placed in a tightly rubber stoppered glass vial as shown in Fig. 4.

For irradiation purposes, the stainless steel "boat" containing the dried sample was put in a glass bottle. The glass bottle was then tightly sealed with aluminum foil and capped with a cap through which a hole had previously been drilled (see Figs. 5-6). To fix the location of the bottle in the irradiator the bottles were inserted in the cells of a plastic sample holder. The plastic sample holder was centered in the "Gammacell" chamber

**THIS BOOK
CONTAINS SEVERAL
DOCUMENTS THAT
ARE OF POOR
QUALITY DUE TO
BEING A
PHOTOCOPY OF A
PHOTO.**

**THIS IS AS RECEIVED
FROM CUSTOMER.**



Fig. 4. View of a rubber stoppered glass vial containing the sample.



Fig. 5. View of the glass bottle with aluminum foil seal, sample, and cap with drilled hole before irradiation.

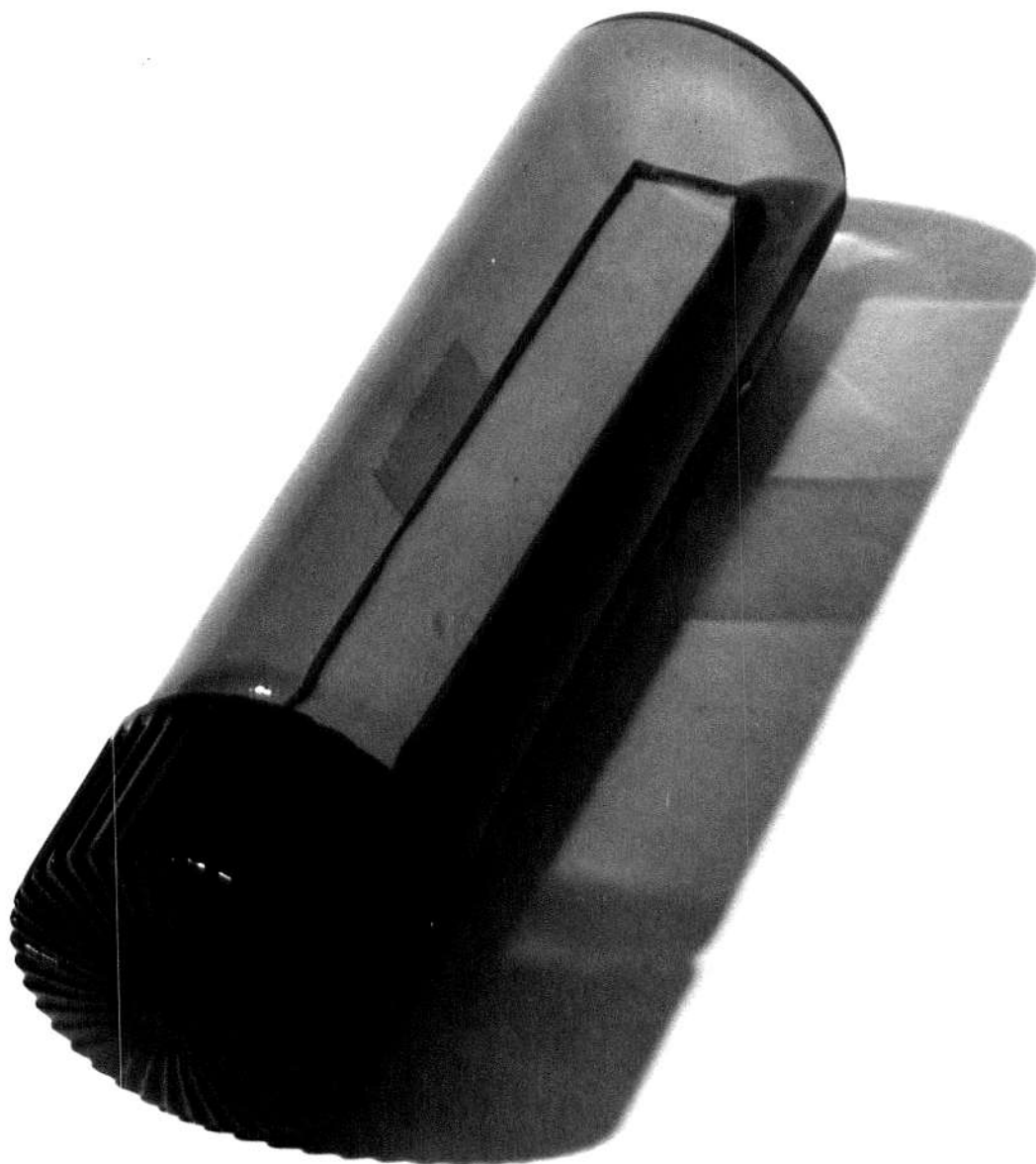


Fig. 6. View of the capped glass bottle with aluminum foil seal after irradiation in the "Gammacell."

during irradiation. The above procedure was followed for irradiation of both calcium carbonate and Kapitzke concrete with gamma radiation. In addition the Kapitzke concrete was subjected to reactor radiation. In this case sealed plastic bottles containing the Kapitzke concrete were placed in one of the thimbles of the rotary specimen rack of the KSU TRIGA Mark II Reactor.

A schematic diagram of the system used for thermal decomposition of calcium carbonate and Kapitzke concrete is shown in Fig. 7. In each experiment an unirradiated and/or irradiated sample in its stainless steel "boat" was centered in the isothermal region (2.25 inches in length) of the high temperature furnace inside a stainless steel tube as shown in Fig. 5. The carbon dioxide released due to thermal decomposition of the sample was carried from the stainless steel tube through copper tubing to the gas chromatograph by helium gas flowing at 4-5 ml/min. The chromatograph injection system was then used to inject 1 cm^3 samples from the flowing stream into the chromatograph for carbon dioxide analysis. The time between two successive injections was two minutes. This sampling and analysis procedure was followed for one hour or until the completion of decomposition.

The operating conditions of the 90-P3 gas chromatograph were as shown in tables 1-2 following.

Table 1. Operating conditions for the Column
and Detector in 90-P3 Gas Chromatograph.

Operating Parts	Transformer Settings	Temperature
Column	Dial on 34	290 °F
Detector	Dial on 17	170 °F

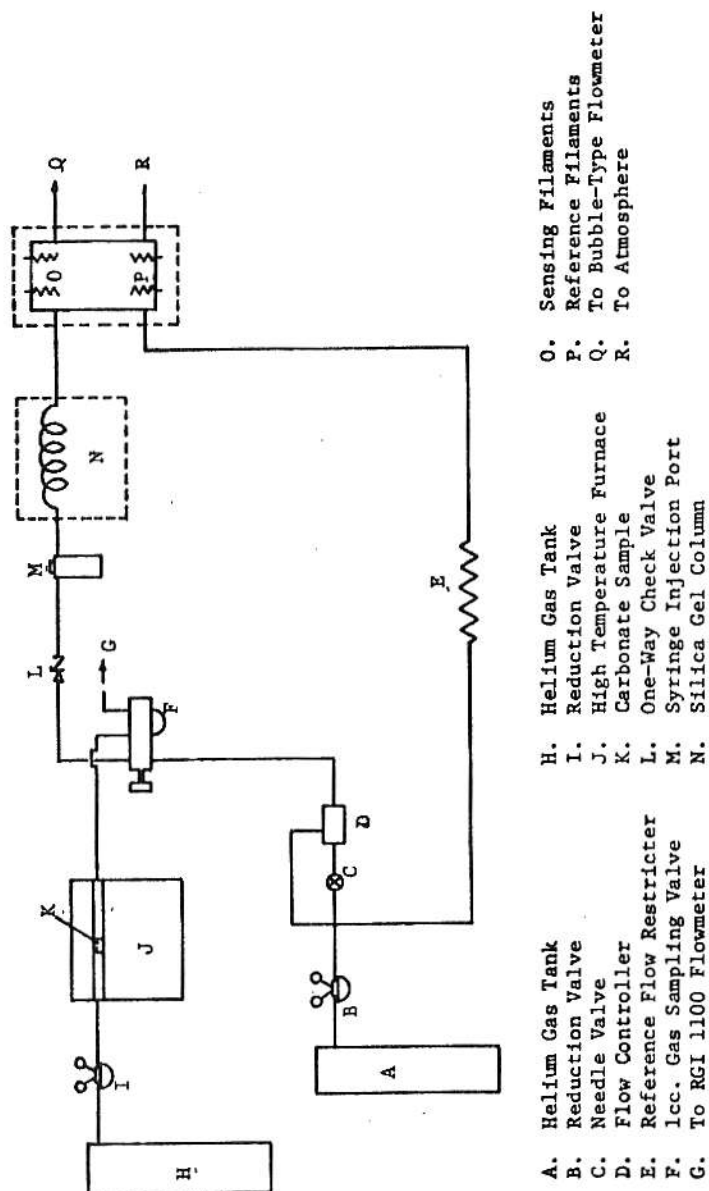


Fig. 7. Schematic diagram of thermal decomposition system.

Table 2. Operating conditions for carrier gas, filament, and attenuator in 90-P3 Gas Chromatograph.

Operating Parts	Scale Reading	Equivalent Reading
Carrier gas (helium)	30.05	50 ml/min.
Filament Current Meter		200 mA
Attenuator	Dial on 32	

The gas chromatograph was absolutely calibrated for the equivalent measure of carbon dioxide gas in a helium-carbon dioxide gaseous mixture. A detailed description of the method is given in Appendix A.

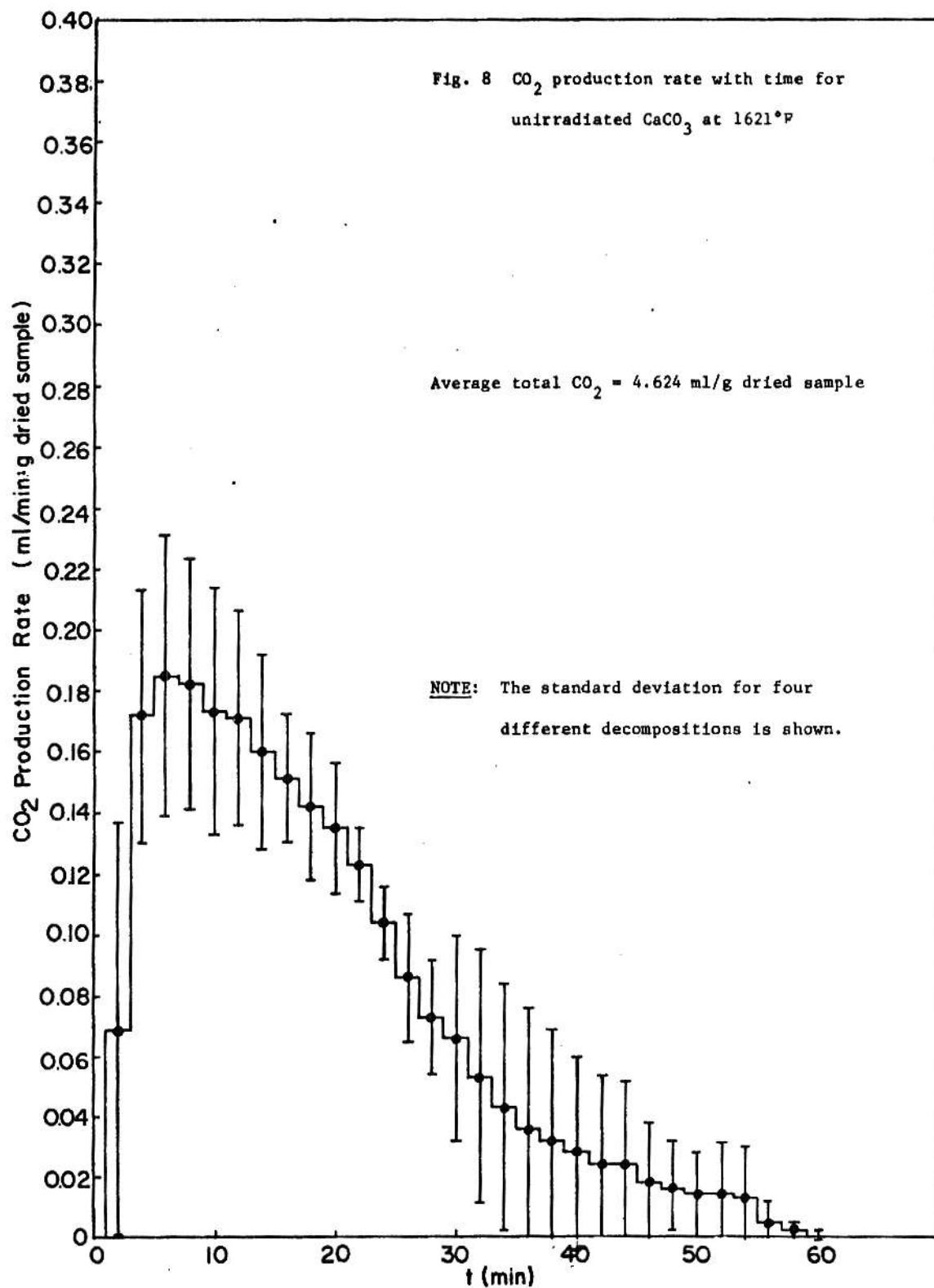
Analysis was made of the atmospheres present in the bottles used to hold samples prior to thermal decomposition both unirradiated and irradiated samples. In this procedure, 1 cm³ samples of the atmosphere in the bottles were taken with a gas tight syringe and injected into the chromatograph for analysis of the carbon dioxide content.

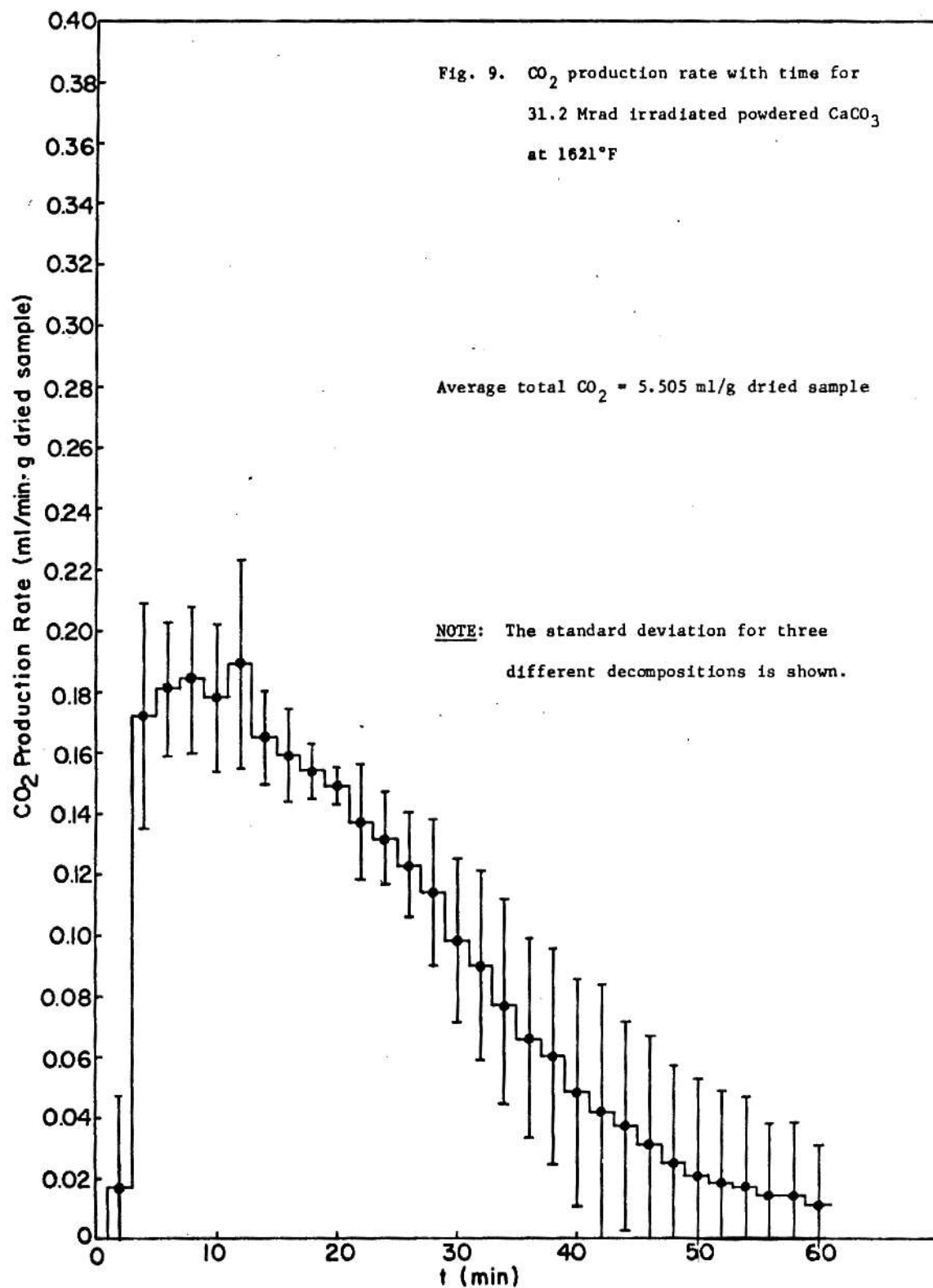
5.0 PRESENTATION OF DATA

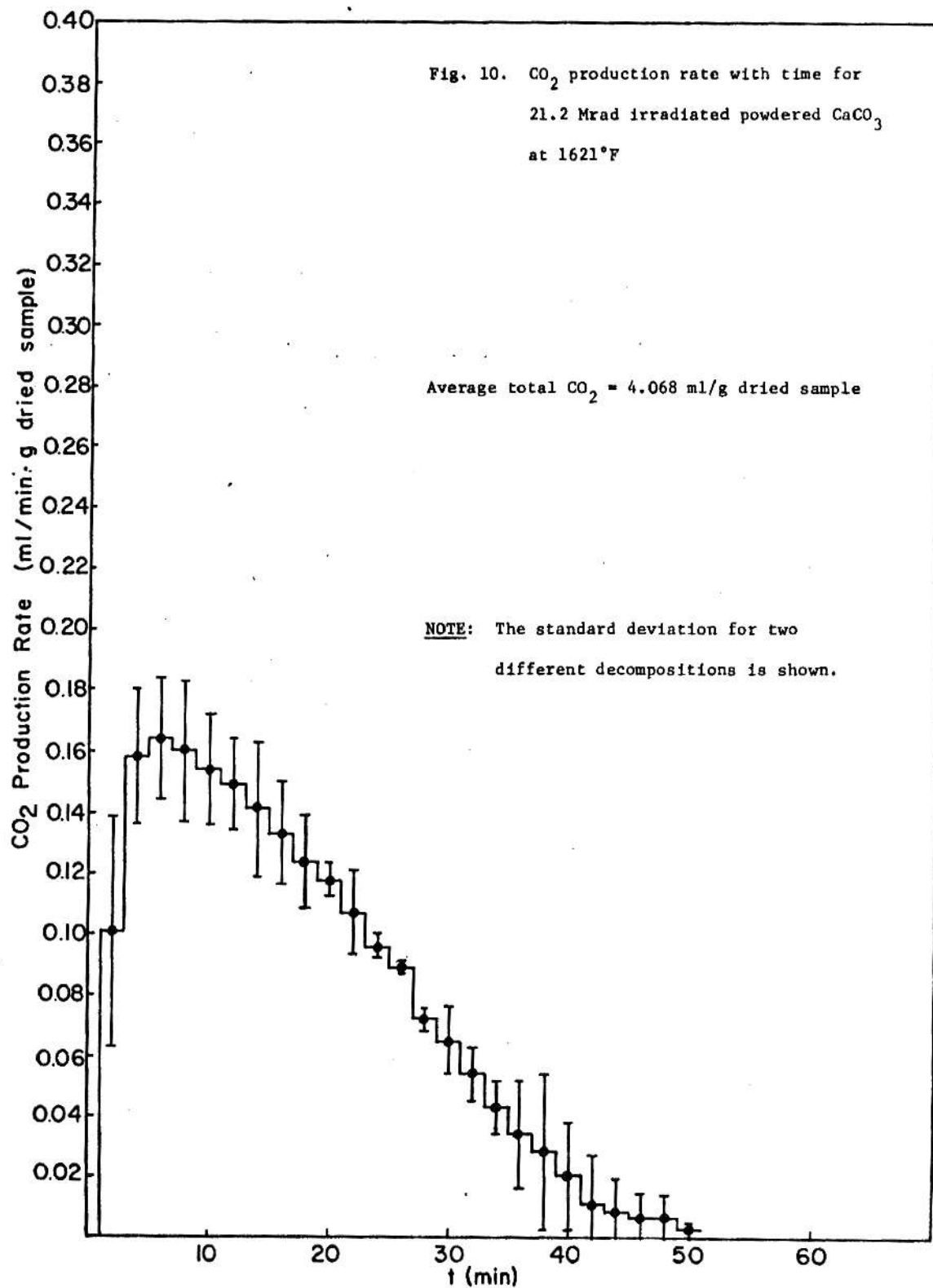
Unirradiated powdered calcium carbonate was thermally decomposed at 1621 °F. Powdered calcium carbonate samples were subjected to radiation doses of 16.03 Mrad, 21.2 Mrad, and 31.2 Mrad of gamma radiation prior to decomposition. A quantitative analysis of the carbon dioxide content was performed as noted earlier and the volume of CO_2 produced by the decomposition was converted to mole percent carbon dioxide using the absolute calibration curve of Appendix A. The carbon dioxide flow rate was determined using the mole fraction carbon dioxide in the sample carrier gas, i.e., the computed mole fraction from the calibration curve, multiplied by the flow rate of the sample carrier gas. The flow rate of carbon dioxide was divided by the initial dry weight of powdered calcium carbonate to obtain the carbon dioxide production rate as a function of time (ml/min·g dried sample). Graphs of the carbon dioxide production rate vs. time were plotted in the form of histograms at the decomposition temperature, 1621 °F, as shown in Figs. 8-11.

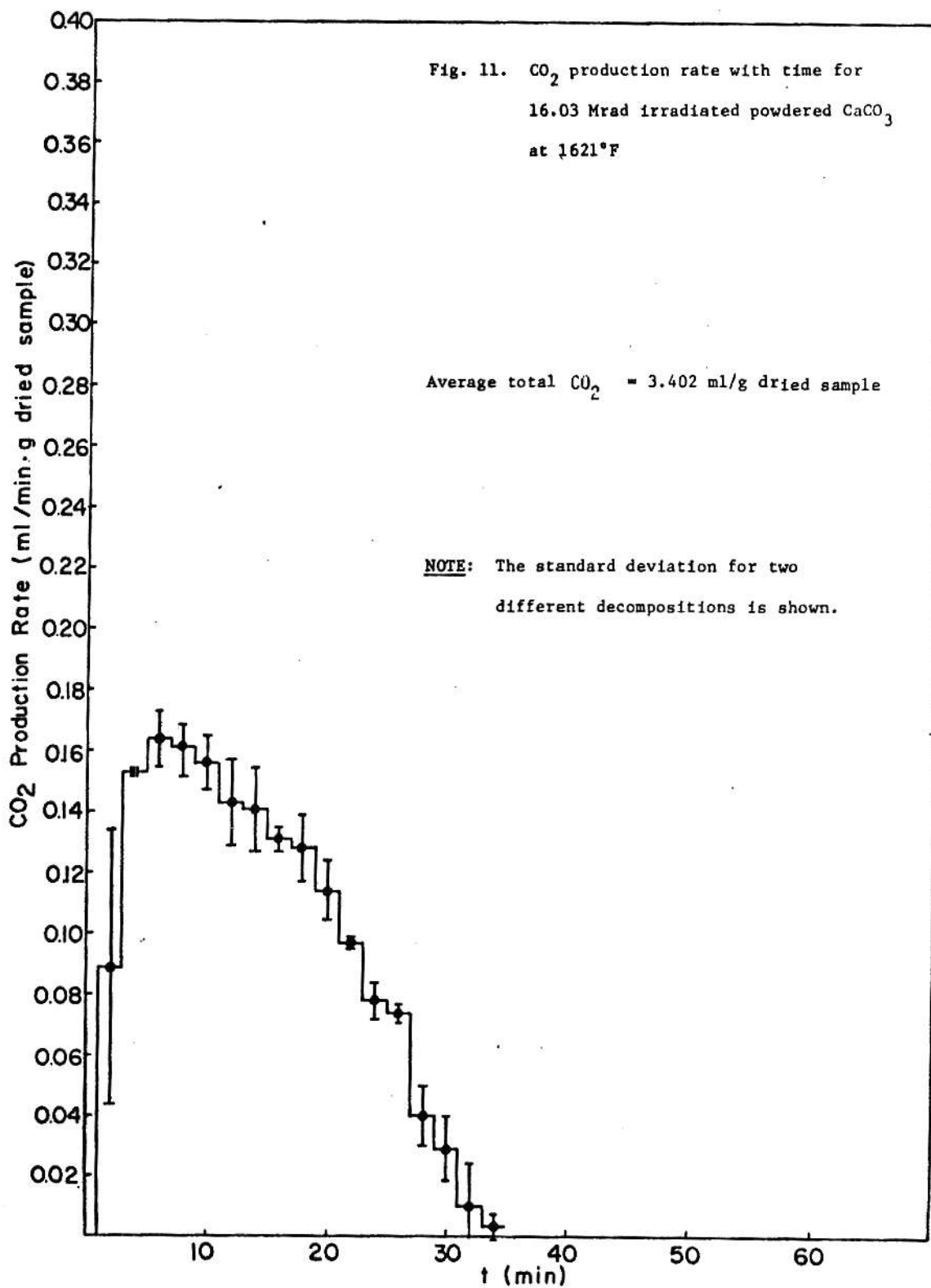
Samples of unirradiated and irradiated powdered Kapitzke concrete were studied in a similar treatment. Powdered Kapitzke concrete samples were subjected to radiation doses of 12.2 Mrad and $54.95 \times 10^{16} \frac{\text{n}}{\text{cm}^2}$, 24.7 Mrad and $11.11 \times 10^{18} \frac{\text{n}}{\text{cm}^2}$, and 19.93 Mrad prior to decomposition at 1621 °F. Histograms of carbon dioxide production rate for the concrete at the decomposition temperature are shown in Figs. 12-15.

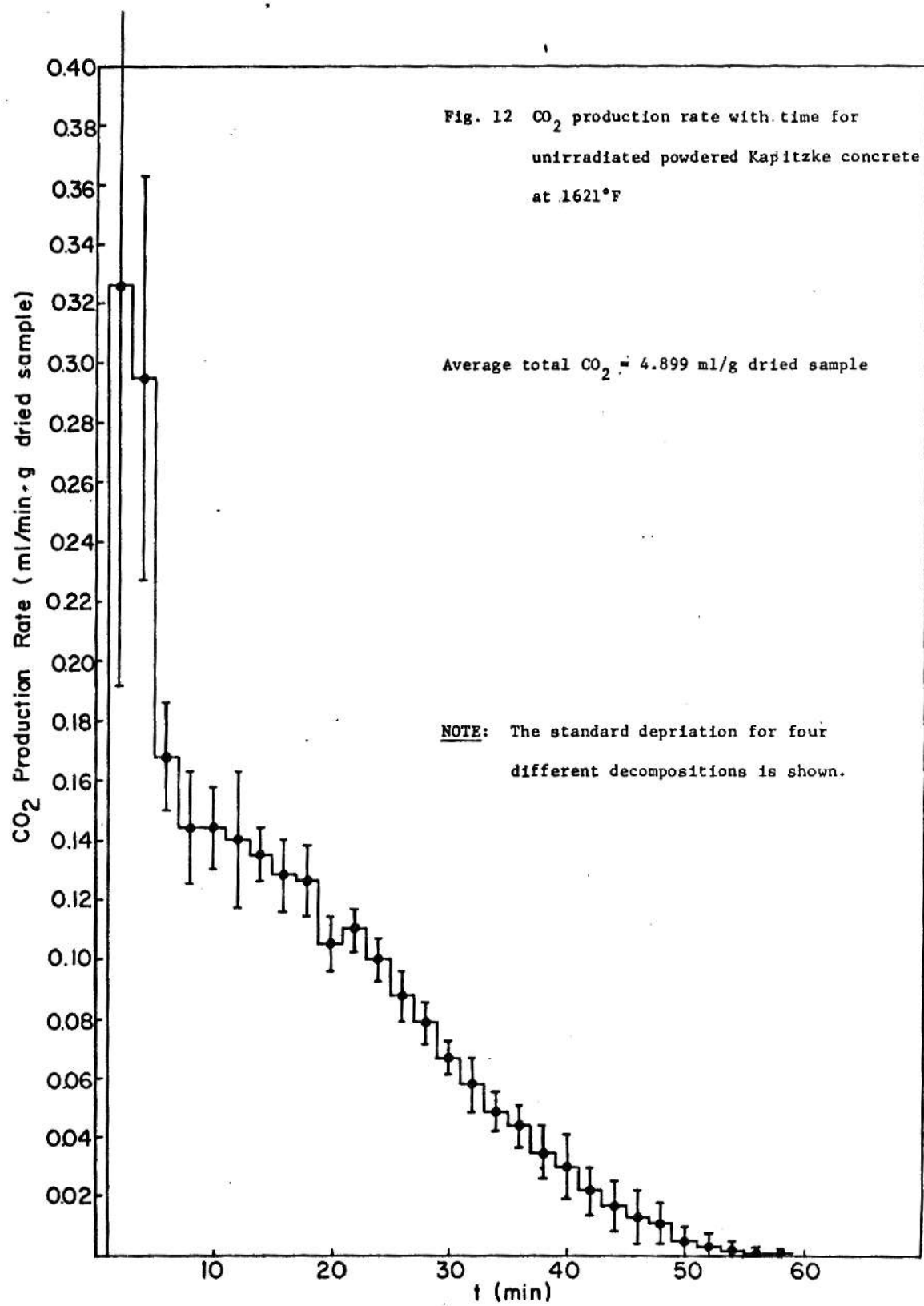
All results are also presented in tabular form in Appendix C for both powdered calcium carbonate and Kapitzke concrete.

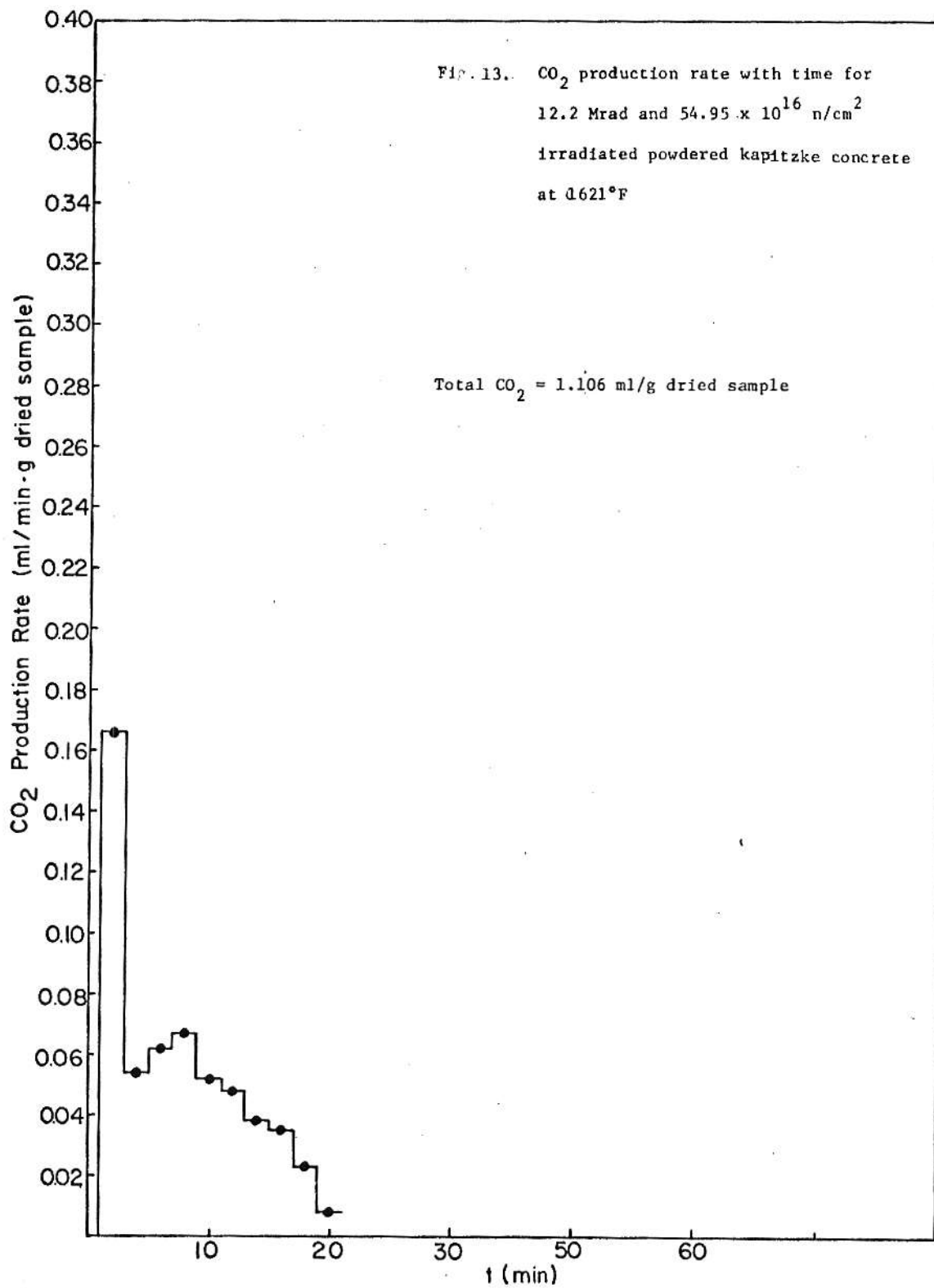


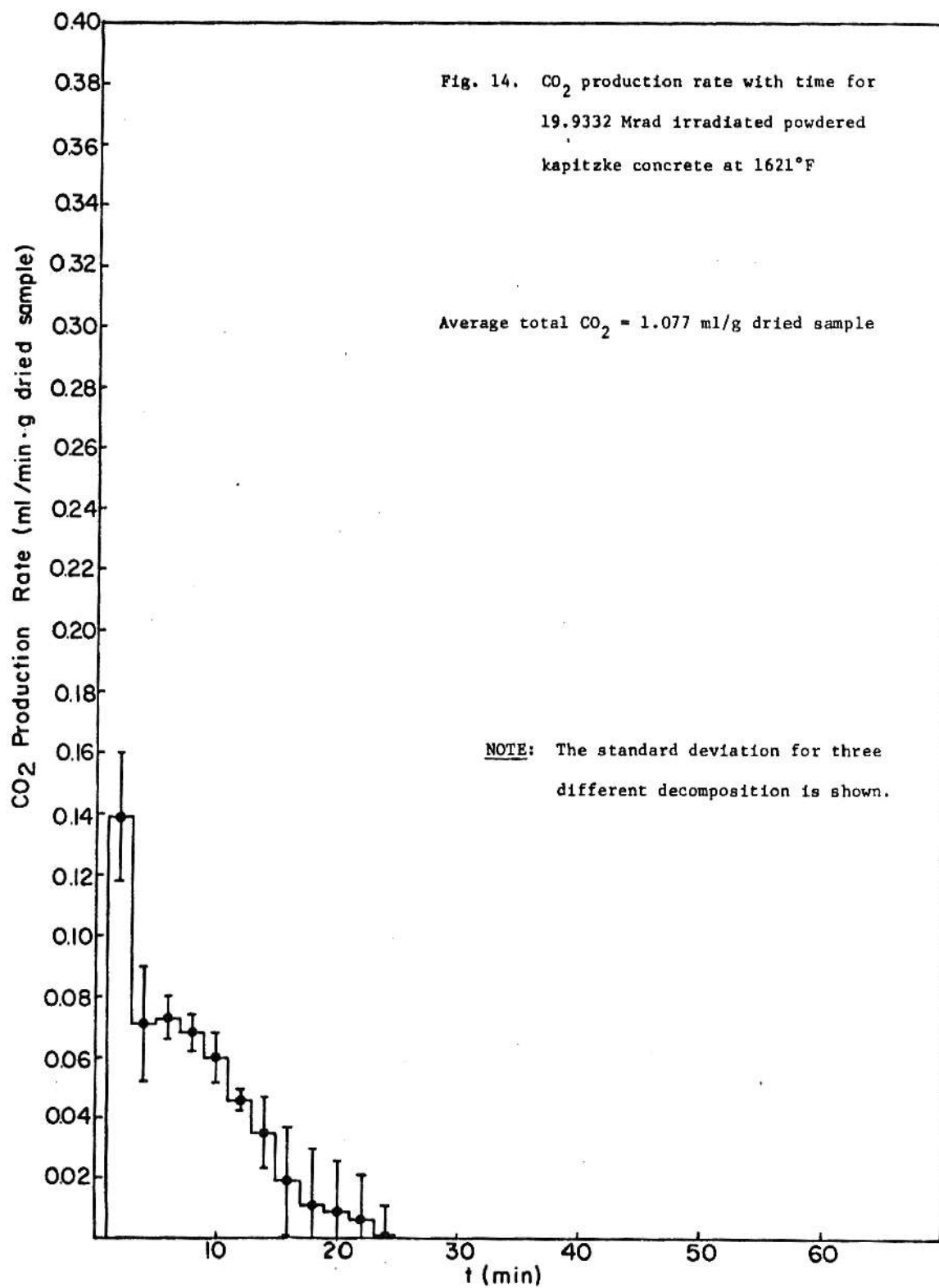


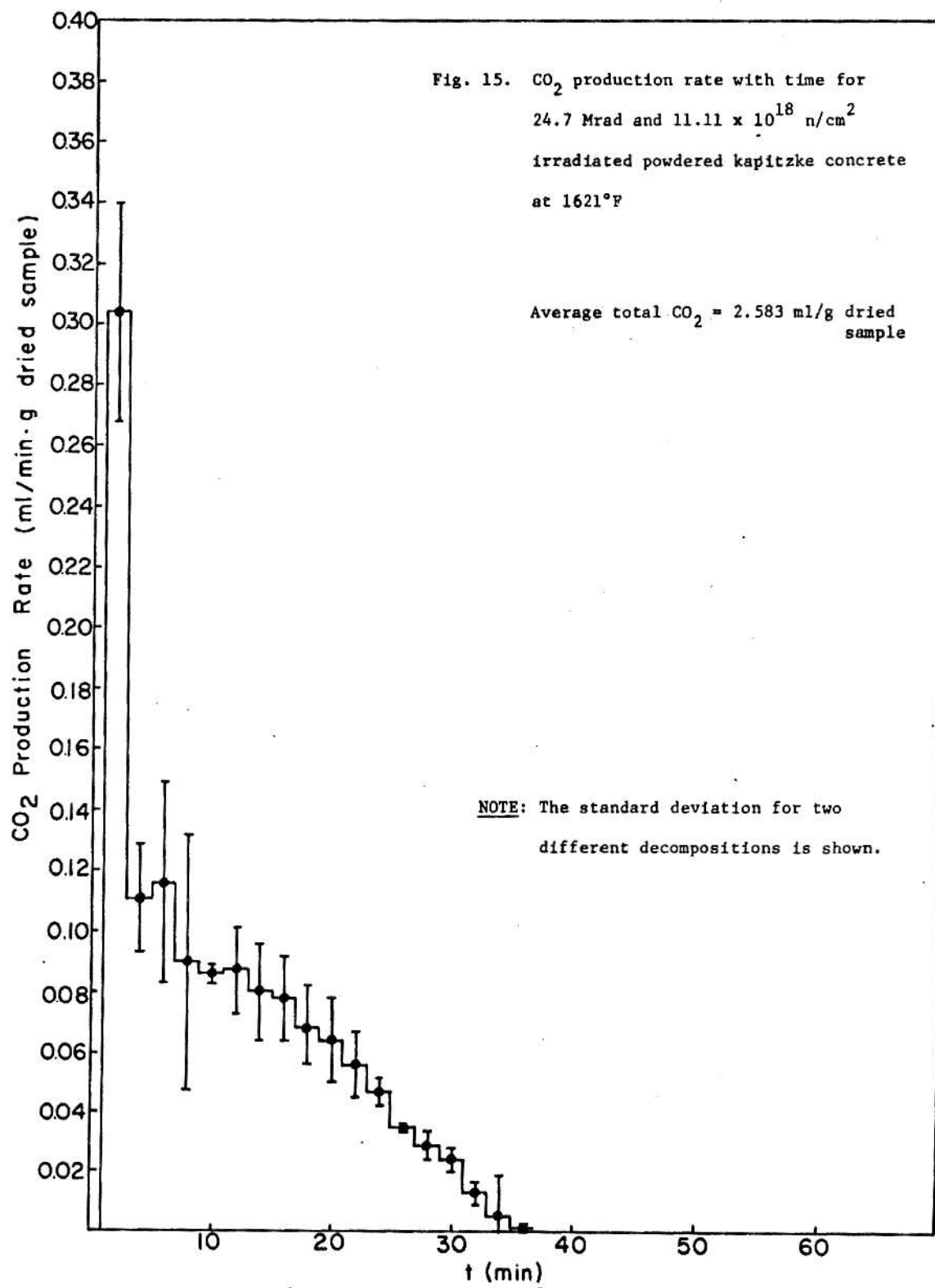












6.0 Discussion of Results and Conclusions

1. The carbon dioxide production rate as a function of time for powdered calcium carbonate exhibits a rapid rise to a maximum rate in the first ten minutes of decomposition. This behavior can be related to a rapid initial decomposition of the surface of the carbonate and mixing of the carbon dioxide with helium carrier gas stream. This behavior is in good agreement with the A portion (initial evolution of gas) of the isothermal decomposition curve (Fig. 1). After the initial rapid rise, the carbon dioxide production rate exhibits a gradual decline from the maximum. This behavior can be ascribed to completion of decomposition at the surface of the carbonate particles. Similar results were obtained with powdered Kapitzke concrete, except in this case the maximum in the CO_2 production rate was obtained within the first two minutes after initiating decomposition.

2. The powdered calcium carbonate and Kapitzke concrete showed no evidence of reduction in carbon dioxide diffusion rate due to sintering or formation of hindrances to flow in the pores between the powder particles. This conclusion is based on the uniform gradual decline of the carbon dioxide rate as shown in Figures 8-15. If the process were diffusion limited it would be expected that the gas evolution curve would rise to a maximum and then hold at the maximum to produce a plateau over a significant period of time.

3. Powdered calcium carbonate during decomposition at 1621 °F was found to shrink and exhibit surface granulation. This shrinkage can be attributed to the presence of the metallic oxide, CaO , which crystallizes

into a sodium chloride type structure after decomposition of hexagonal crystals of the CaCO_3 . Similar results were obtained with heated powdered Kapitzke concrete. A photograph of a heated powdered calcium carbonate sample is shown in Figure 16. Granulation and shrinkage is evident in the photograph.

4. The carbon dioxide production rate, expressed as volume per unit weight of dried sample prior to decomposition, was used to obtain an indication of the uniformity of packing of the sample, its composition and size of the sample particles. According to this criterion, it was found that the total carbon dioxide produced per unit weight of the dried sample exhibited a deviation from the average value of from 5.8 to 28.1% for powdered calcium carbonate and from 4.6 to 15.8% for powdered Kapitzke concrete. These deviations indicate probable non-uniformity in the composition and size of the sample particles and/or in the vibrational packing of the sample prior to heating and decomposition.

5. Compared with unirradiated samples thermal decomposition of calcium carbonate irradiated with Co-60 gamma-ray radiation and Kapitzke concrete irradiated with Co-60 gamma-ray radiation and both KSU TRIGA reactor gamma-ray radiation and neutrons, show an initial decrease in carbon dioxide production and then increasing production with increasing dose (see Figs. 8-15). This observation was based on the first ten minutes of sample decomposition of calcium carbonate and on the first two minutes of sample decomposition of Kapitzke concrete. This effect can be related to the deposit by gamma-radiation and/or neutron radiation, of energy in the sample which produces damage to the crystal structure. This conclusion is based on the observation that neutron irradiation causes significant changes in the physical and mechanical properties of concrete, its component aggregates and its cement paste (21).



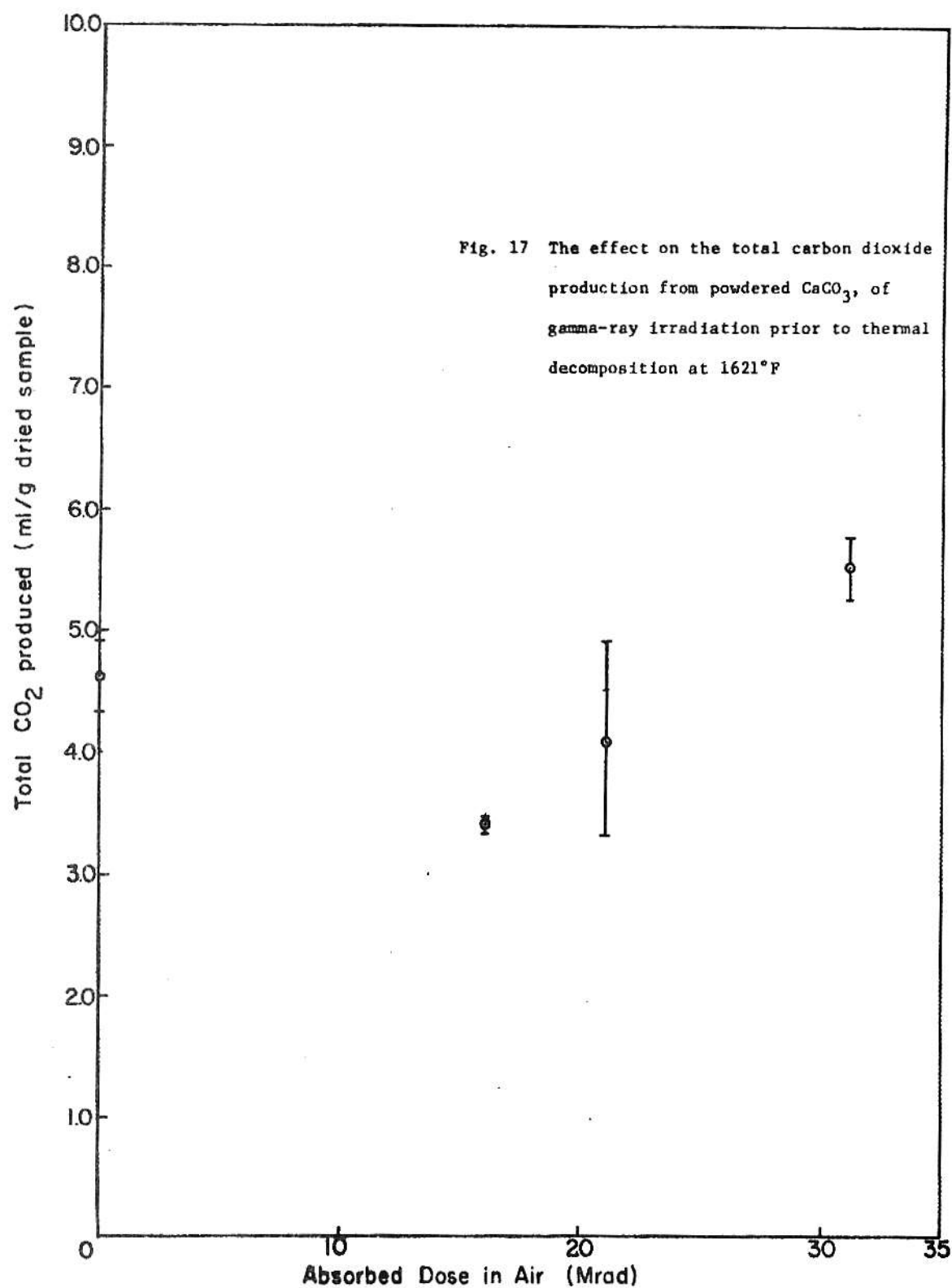
Fig. 16. View of the powdered calcium carbonate
heated for one hour at 1621°F

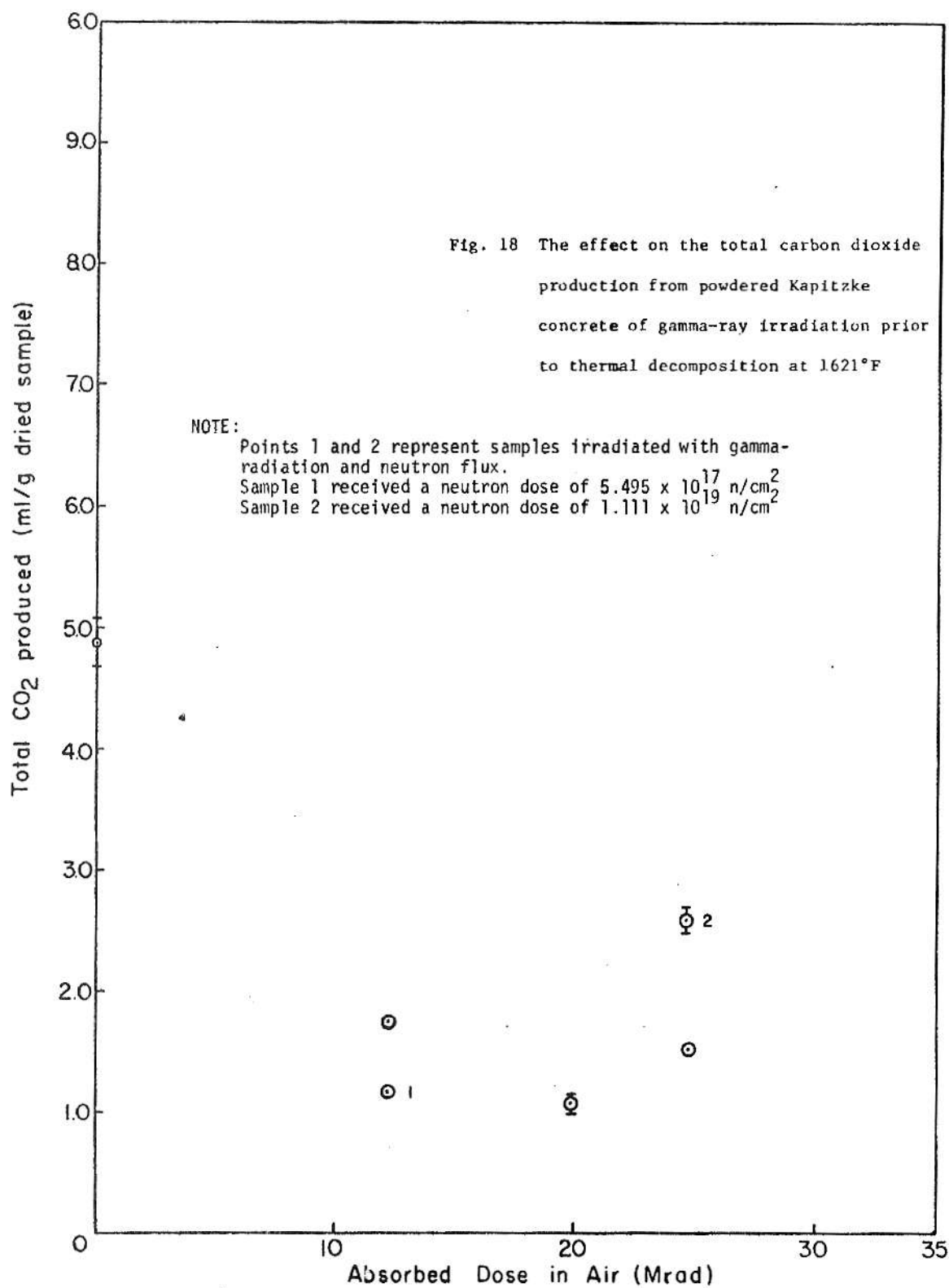
For both types of samples it is observed that as the gamma-ray radiation dose increases, the susceptibility to thermal decomposition passes through an apparent minimum and then begins to increase. For CaCO_3 at a dose of about 30 Mrad the external decomposition is significantly above that noted for the unirradiated material. This behavior may result from eventual break down of the thermal decomposition resistant structure with increasing radiation dose. Neutron and gamma-ray irradiation of Kapitzke concrete samples (gamma dose 12.2 Mrad; neutron fluence, 5.5×10^{17} neutrons/cm²)* showed, compared to samples receiving the same gamma-ray dose (from Co-60) a further decrease in carbon dioxide production compared to unirradiated samples. However with an increase in gamma-ray dose and neutron fluence, the carbon dioxide production rate increased over that noted at the same gamma-ray dose in the absence of the neutron fluence (gamma dose, 24.7 Mrad; neutron fluence, 1.11×10^{19} n/cm²). The effects of gamma-ray and neutron irradiation appear to be additive in terms of the effect on the rate of carbon dioxide production.

A graphical representation of the total carbon dioxide production versus gamma radiation dose is shown in Figures 17-18 for both powdered calcium carbonate and Kapitzke concrete.

6. Gas chromatographic analysis of the atmosphere in the bottles in which the powdered calcium carbonates were irradiated showed only trace quantities of carbon dioxide similar to that present normally in the atmosphere. Analysis of the atmospheres in bottles in which unirradiated powdered calcium carbonate samples were enclosed for times equivalent to the irradiation times, showed no carbon dioxide release above that present in the atmosphere.

*The fluences noted in the text and graphs are thermal neutron values; fast fluence is about an order of magnitude lower (22).





Thus calcium carbonate does not spontaneously decompose to a detectable degree at 68°F. Chromatographic analysis of the atmospheres present in irradiated and unirradiated bottles, in which powdered Kapitzke concrete were enclosed showed no carbon dioxide release in either case. Thus the decomposition of powdered Kapitzke concrete due to the irradiation or due to spontaneous decomposition at 68°F temperature was not present to a detectable extent.

7. It is expected that many of the questions raised by this research could be answered if a determination of what and the relative amount of the various compounds present in unirradiated and irradiated concrete samples could be determined. It is known that this type of analysis can be carried out with difficulty using X-ray diffraction patterns. This technique, determines by comparison of an X-ray photograph or diffractogram for the sample substance with a library of diffractograms of known substances the substances and the relative amounts present. X-ray diffraction procedures presented in Appendix B, can be used for concrete analysis but because of the extreme difficulty inherent in applying this technique when only subtle changes are occurring in composition, it was not practical to apply this procedure in this study.

8. The fractional decomposition, α , was calculated using two different methods. In the first method, α was calculated from a knowledge of C_i as follows:

$$C_i = \frac{V_i MP}{RT}$$

where C_i = weight of carbon dioxide released (g) in each time period (2,4,6,8,...)

V_i = Volume of carbon dioxide released (ml) in each time period (2,4,6,8,...)

M = Molecular weight of carbon dioxide (44 g/mole)

P = Atmospheric pressure (1 atm)

R = Gas constant (82 ml. atm/mole.°K)

T = Absolute temperature (°K)

i = Time intervals (2,4,6,8,10,...)

and

$$\alpha = \frac{C_1(g)}{K W_0(g)}$$

where K = The fraction of sample weight which is CO₂ (0.44 for CaCO₃ and 0.2161 for Kapitzke concrete)

α_1 = Fractional decomposition in time i (dimensionless)

W₀(g) = Initial weight of the solid sample (g)

i = Time interval (2,4,8,10,...)

The cumulative value of α for the time periods, 2 to n is

$$\alpha = \sum_{i=2}^n \alpha_1$$

$$n = 2,4,6,8,\dots$$

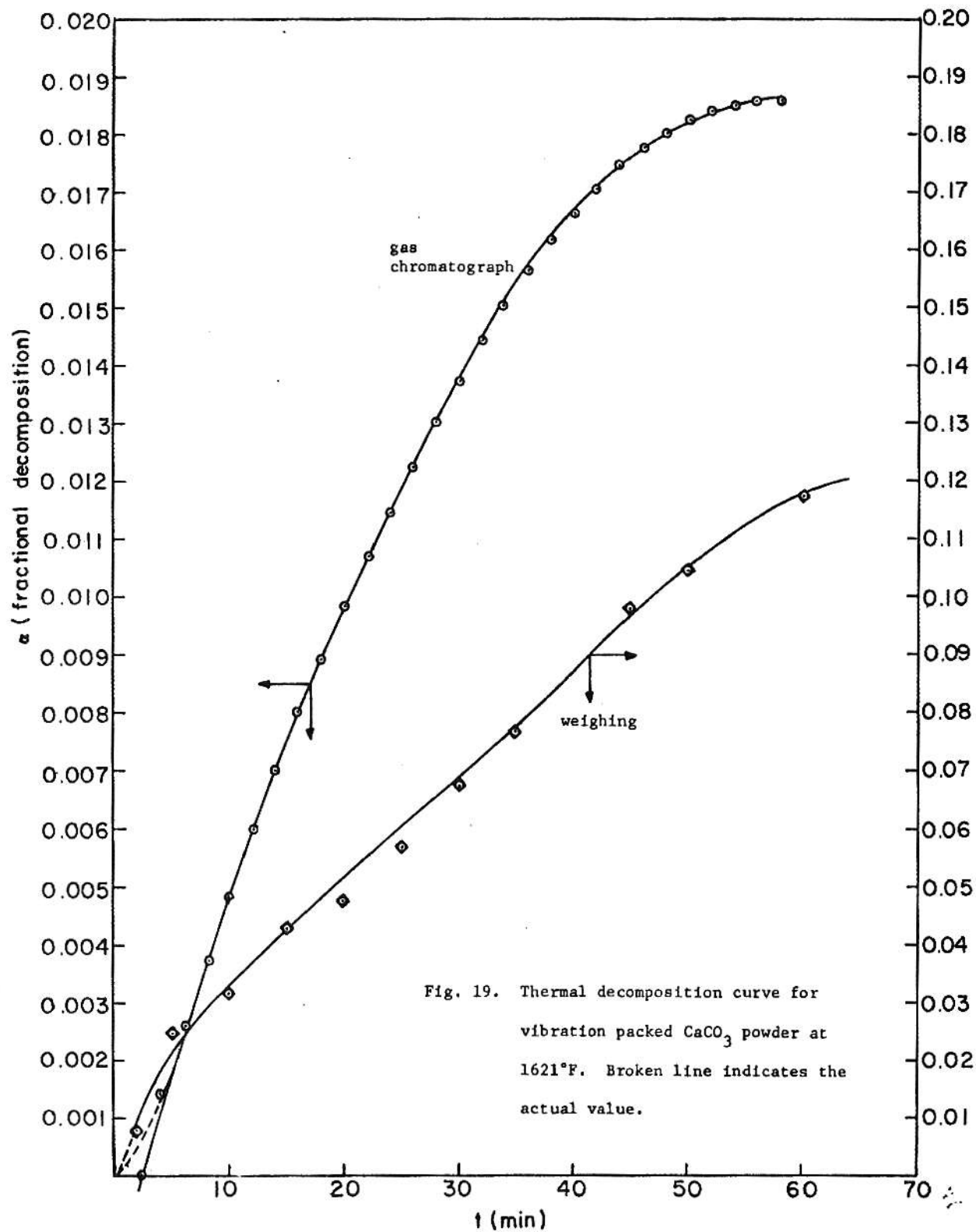
In the second method, α was calculated for both calcium carbonate and Kapitzke concrete according to the following procedure:

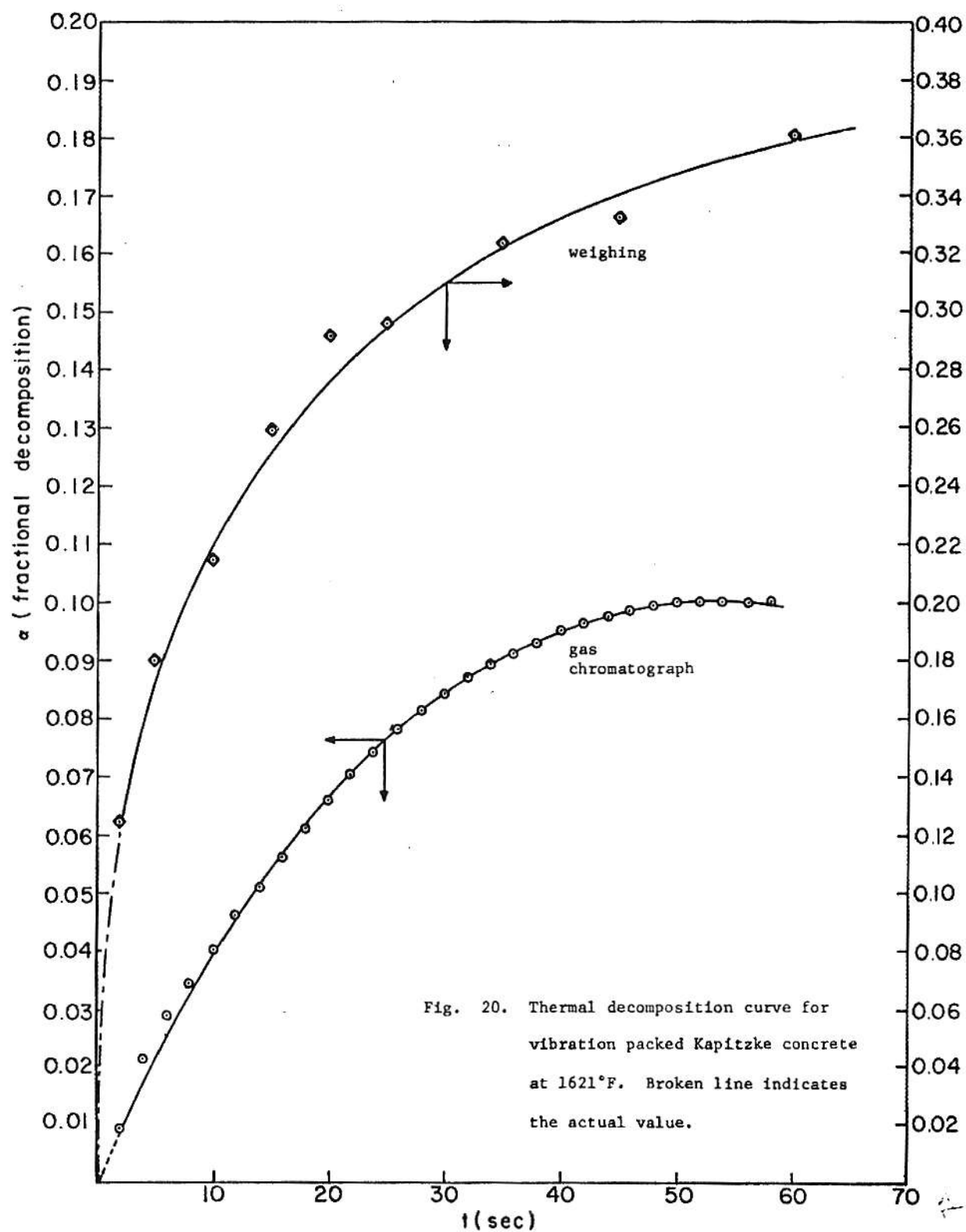
- (a) A carbonate or concrete sample was heated for different time periods (2,5,10,15,20,...60 minutes) at 1621°F and w₁, the weight of the sample at time i, measured.
- (b) α , the fractional decomposition was then determined as

$$\alpha = \frac{W_o - W_i}{AW_o}$$

where W_o = Initial weight of solid sample (g)
 W_i = The weight of the sample at time $i = 2, 5, 10, 15, \dots 60$ minutes.
 A = The fraction of sample weight which is CO_2 (0.44 for $CaCO_3$
 and 0.1324 for Kapitzke concrete (Appendix D)).

Comparison of values of α calculated by the two methods exhibited a difference; the values of α determined by the first method were in all cases less than those obtained by the second. The difference in the two results can be explained if it is assumed with respect to the sample subjected to the second method that during the weighing process when a sample was cooled to room temperature, weighed and then reheated to 1621°F, surface decomposed material (CaO) cracked and exposed a new $CaCO_3$ material which subsequently decomposed during further heating cycles. Since the cubic CaO and hexagonal $CaCO_3$ crystals had different coefficients of expansion this result would be expected. Values of α calculated by the two methods are plotted in Figures 19 and 20 and are tabulated in Tables 9-10 of Appendix C. (The plots lie in the region of initial gas evolution (see generalized decomposition curve, (Fig. 1)) thus both methods indicate that the thermal decomposition of both calcium carbonate and Kapitzke concrete occurs only at the surface or near surface layers of the powder particles. This conclusion indicates that the interior layers of both the calcium carbonate and Kapitzke concrete particles have a strong structure which resists thermal decomposition once they are coated with decomposition product, i.e. CaO (18).





9. Powdered Kapitzke concrete was mixed with powdered aluminum metal and water in a plastic bottle. Within a period of ten minutes following mixing, a vigorous chemical reaction was observed. Hydrogen gas evolved due to the reaction (equations 1-4) was detected by observing the glow and pop obtained when a wood ember was introduced into the plastic bottle. A similar mixing process was carried out using powdered zinc metal and iron metal. A slow reaction was observed in the mixture containing powdered zinc metal while no detectable reaction was observed in the mixture containing iron metal over a period of several days.

The vigorous chemical reaction in the presence of aluminum indicates that concrete canned in aluminum can produce a high-pressure release due to chemical reaction between concrete and aluminum metal in the presence of water. This observation provides an explanation of the high pressure gas release noted in the beam tube of the Puerto Rico Nuclear Center Research Reactor (16) and to the similar release noted in a radiation shield plug ruptured within an 8" beam tube at 1-MW pool-type reactor facility (17).

7.0 Suggestions for Further Study

In this work, a cutting and weighing integration technique was used to analyze the chromatographic output. This technique is time consuming and therefore it is suggested that an electronic digital integrator capable of fast, precise analysis be purchased and used in future work.

Further work should be performed to study the thermal decomposition of mixtures of calcium or powdered Kapitzke concrete and aluminum metal. Further work should also include a study of calcium carbonate and concrete encapsulated in aluminum containers. The effect of both radiation (gamma-ray and neutron irradiation) and heat on the buildup of gas within the closed containers is worthy of study.

8.0 Acknowledgement

The author wishes to express his deepest appreciation and gratitude to Dr. Walter Meyer under whose direction this study has been accomplished. Sincere appreciation is also extended to Dr. Cecil Best, Dr. Richard E. Faw and Dr. Fred Merklin for their valuable advice during this work. My special gratitude to Dr. Curtis G. Chezem, Head of the Kansas State University Department of Nuclear Engineering and all faculty with whom I have had contact. Thanks are extended to the reactor operator, Mr. Mike McEwan, and to the machinist, Mr. George Abshire. Sincere appreciation is extended to Mr. D. Labelle for his valuable advice. Thanks are extended to the people in the Engineering Typing Center for typing this thesis. Recognition and gratitude should be given to the Government of Iraqi Republic for their financial support during the study period. Sincere gratitude is given to my wife, Nidhal, for her encouragement and invaluable assistance.

9.0 References

1. Measured Fast-Neutron Spectra After Reflection of Fission Source Neutrons From a Nine-Inch-Thick Concrete Slab, Walter Meyer, Gale G. Simons, William R. Kimel (KSU), Trans. Am. Nucl. Soc., 705 (1968).
2. D. W. Labelle, "The Effects of Co-60 Gamma Radiation on the Thermal Decomposition of Carbonate Compounds," (A Master's Thesis), Kansas State University (1969).
3. D. A. Young, "Decomposition of solids The International Encyclopedia of Physical Chemistry and Chemical Physics (Editors: E. A. Guggenheim, J. E. Mayer and F. C. Tompkins), Pergamon Press, London, pp 1-4, 6, 14, 28 (1966).
4. I. Langmuir, "The Dissociation of Solids and the Kinetic Interpretation of the Phase Rule," J. Am. Chem. Soc., 38, 2263 (1916).
5. C. N. Hinshelwood and E. J. Bowen, "The Influence of Physical Conditions on the Velocity of Decomposition of Certain Crystalline Solids," Proc. Roy. Soc., A99, 203-212 (1921).
6. J. Y. MacDonald and C. N. Hinshelwood, "Formation and Growth of Silver Nuclei in the Decomposition of Silver Oxalate," J. Chem. Soc., 127, 2764-2771 (1925).
7. W. E. Garner *et. al.*, "The Dehydration of Ammonium, Potassium and Some Mixed Alums," Proc. Roy. Soc., A189, 508-527 (1947).
8. B. Topley and M. L. Smith, "Kinetics of Salt - Hydrate Dissociations: $\text{MnC}_2\text{O}_4 \cdot 2\text{H}_2\text{O} = \text{MnC}_2\text{O}_4 + 2\text{H}_2\text{O}$," J. Chem. Soc., 321-325 (1935).
9. W. E. Garner and J. A. Cooper, "Dehydration of crystals of chrome Alum," Proc. Roy. Soc., A174, 487-503 (1940).
10. G. J. Dienes and G. H. Vineyard, Radiation Effects in Solids, Interscience Publishers, Inc., 250 Fifth Avenue, New York, I, N.Y., 2(1957).
11. J. J. Harwood, Henry H. Hausner, J. G. Morse and W. G. Rauch, The effects of Radiation on Materials, Reinhold Publishing Corporation, New York, 288 (1958).
12. A. O. Allen and J. A. Ghormley, "Decomposition of Solid Barium Nitrate by Fast Electrons," J. Chem. Phys., 15, 208 (1947).
13. G. Henning, R. Less, and M. S. Matheson, "The Decomposition of Nitrate Crystals by Ionizing Radiations," J. Chem. Phys., 21, 664 (1953).

14. "Calibration Directions for F 1100 Flowmeter," RGI, Inc., Vineland, New Jersey.
15. F. M. Lea, The Chemistry of Cement and Concrete, Bell and Bain Ltd., Glasgow, 690 (1970).
16. High-Pressure Release in an Eight-Inch Tube of the Puerto Rico Research Reactor, The U.S. Atomic Energy Commission, Division of Operational Safety, Operating Experiences, ROE: 66-3 (October 25, 1966).
17. Radiation Shield Plug Overpressurization Hazard, The U.S. Atomic Energy Commission, Division of Operational Safety, Serious Accidents, Issue No. 295 (December 9, 1968).
18. H. T. S. Britton, S. J. Gregg and G. W. Winson, "The Thermal Decomposition of Dolomite," Trans. Faraday Soc., (1952) 48, 70.
19. Personal Communication, R. L. Henderson, Monarch Cement Company, Humboldt, Kansas to Dr. Cecil H. Best (December 2, 1972).
20. Personal Communication, Tom Murphy, Ash Grove Cement Company, Kansas City, Kansas to Dr. Cecil H. Best (October 22, 1971).
21. M. F. Elleuch, F. Dubois and J. Rappeneau, "Behavior of Special Shielding Concretes and Their Components Under Neutron Irradiation," Commissariat a l'Energie Atomique, Saclay, France, 40-3 (April 1971).
22. G. D. Bouchey, "Experimental Neutron Flux Measurements and Power Calibration in The Kansas State University TRIGA Mark II Nuclear Reactor" (A Master's Thesis), Kansas State University (1967).

10.0 Appendices

APPENDIX A

The Calibration of the 90P3 Gas Chromatograph

According to the procedure described below, the 90P3 Varian gas Chromatograph was absolutely calibrated for the quantitative analysis of carbon dioxide in a helium carrier gas. The purpose of the calibration was to provide a graphical relation between known concentrations of carbon dioxide in a helium-carbon dioxide mixture and the corresponding weights of the integrated chromatographic output.

The method used for calibration was as follows:

(1) Known concentrations of carbon dioxide and helium gas were prepared from commercial compressed gas cylinders using suitable gas regulators and flow meters. The flow rates of the standard carbon dioxide and helium gas were separately measured using an RGI-F1100 flowmeter (19) (the calibration curves of the flowmeter are presented in Fig. 1A). The two gases were then mixed together and passed to the injection system on the gas chromatograph through a tubing arrangement as shown in Fig. 2A.

(2) The chromatographic output was obtained in the form of Gaussian-shaped peaks for carbon dioxide on a 1 mV scale strip chart recorder. Peak areas were determined by cutting out the chromatographic peak and weighing the paper on an analytical balance (2). Peak weights with corresponding mole fractions of carbon dioxide are given in Table 1-A. A graph of peak weight vs. mole fractions of CO_2 , using a linear least squares fit, is also attached (see Figure 3A). This plot was used to compute the mole fraction of CO_2 corresponding to the peak weight in each run. The same procedure was used for the following runs except that the data of each run were multiplied by

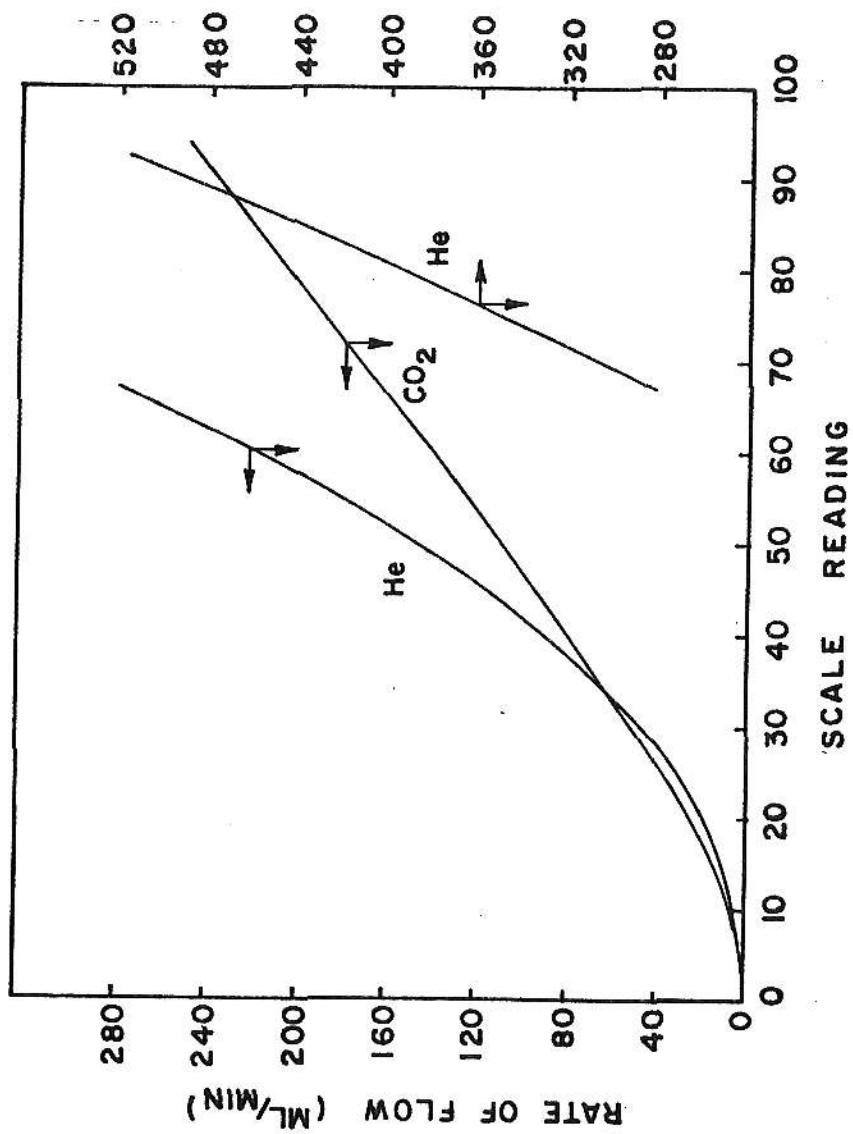


Fig. 1A Helium and carbon dioxide calibration curves for RGI-F1100 flowmeter.

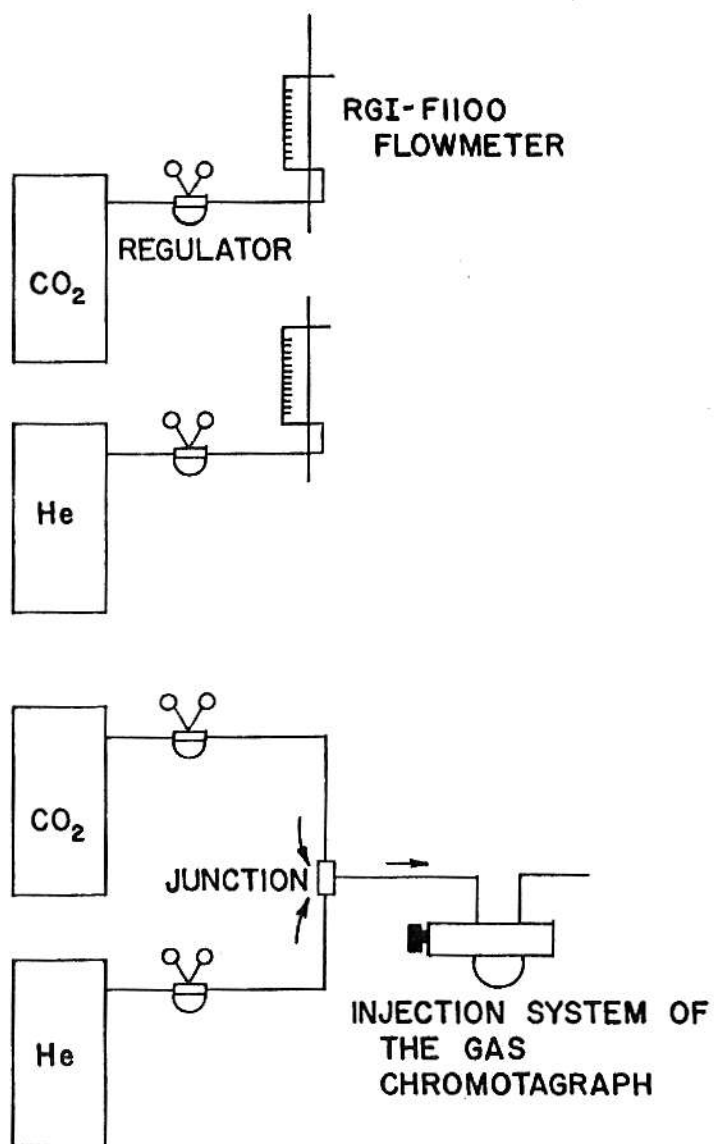


Fig. 2A Schematic diagram of tubing arrangements

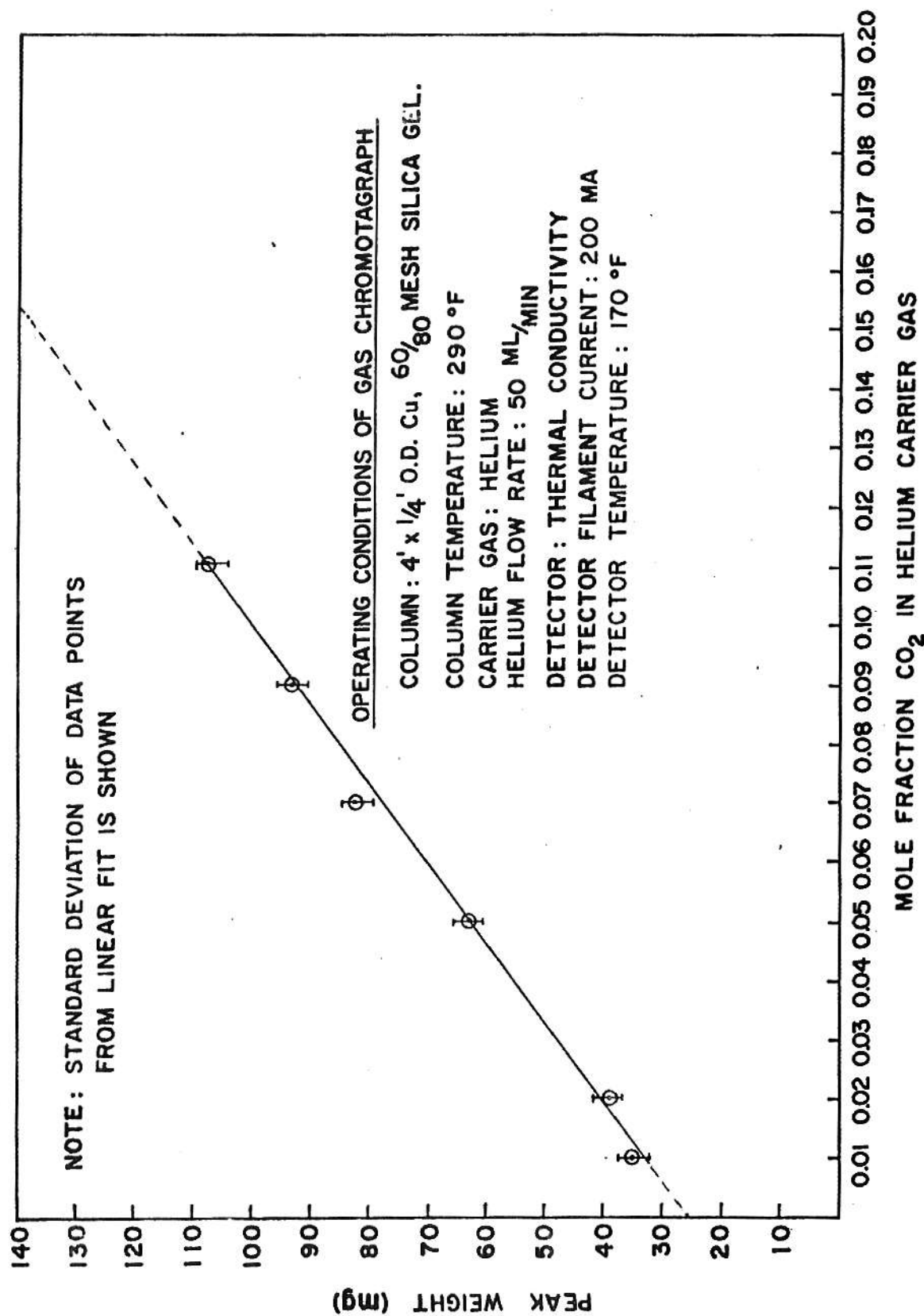


Fig. 3A. Calibration curve for helium mixture with 0.0 - 0.11 mole fraction CO₂ for 90 P3 gas chromatograph

the ratio A_{II}/A_I

where $A_I = W_\ell(g)/W_s(g)$ for the previous run

$A_{II} = W_\ell(g)/W_s(g)$ for the following run

for normalization purpose.

Table 1-A. Data for the Calibration of the 90P3

Chromatograph for Carbon Dioxide.

CO ₂ Content of CO ₂ -Helium Mixture (mole fraction)	Peak Weight (mg)
0.01	35.00
0.02	38.90
0.05	62.84
0.07	81.92
0.09	93.30
0.11	106.36

APPENDIX B

The Powder X-ray diagram

In this technique (15) a sample in powder form is placed at the center of a cylindrical camera and irradiated by a beam of X-rays as in Fig. 1B. Each set of planes (hkl) in the crystal can produce a diffracted beam. This is true only if that set of planes is at an angle θ to the primary beam defined by the equation

$$d_{hkl} = \frac{n\lambda}{2 \sin\theta}$$

where d_{hkl} = the interplanar spacing distance.

(hkl) = the Miller indices

θ = an angle of incidence.

λ = X-ray wave length

n = an integer number

(1,2,3 ... etc.)

If the crystal is turned about at random in the beam, reflected beams will appear as the critical values of θ are passed. All these reflected beams will form cones whose apices are the crystal and which cut across the photographic film to give arcs from which the angle θ and the spacings $\frac{d}{n}$ can be found. If the relative intensity of each arc is also recorded, the resulting table of spacings and intensities is characteristic of the substance under examination.

The American Society for Testing and Materials (15) has compiled an Index of X-ray data in which substances are classified according to the spacings of three strongest lines in the powder X-ray diagram. X-ray data are given below for all the substances of interest in cement chemistry, the

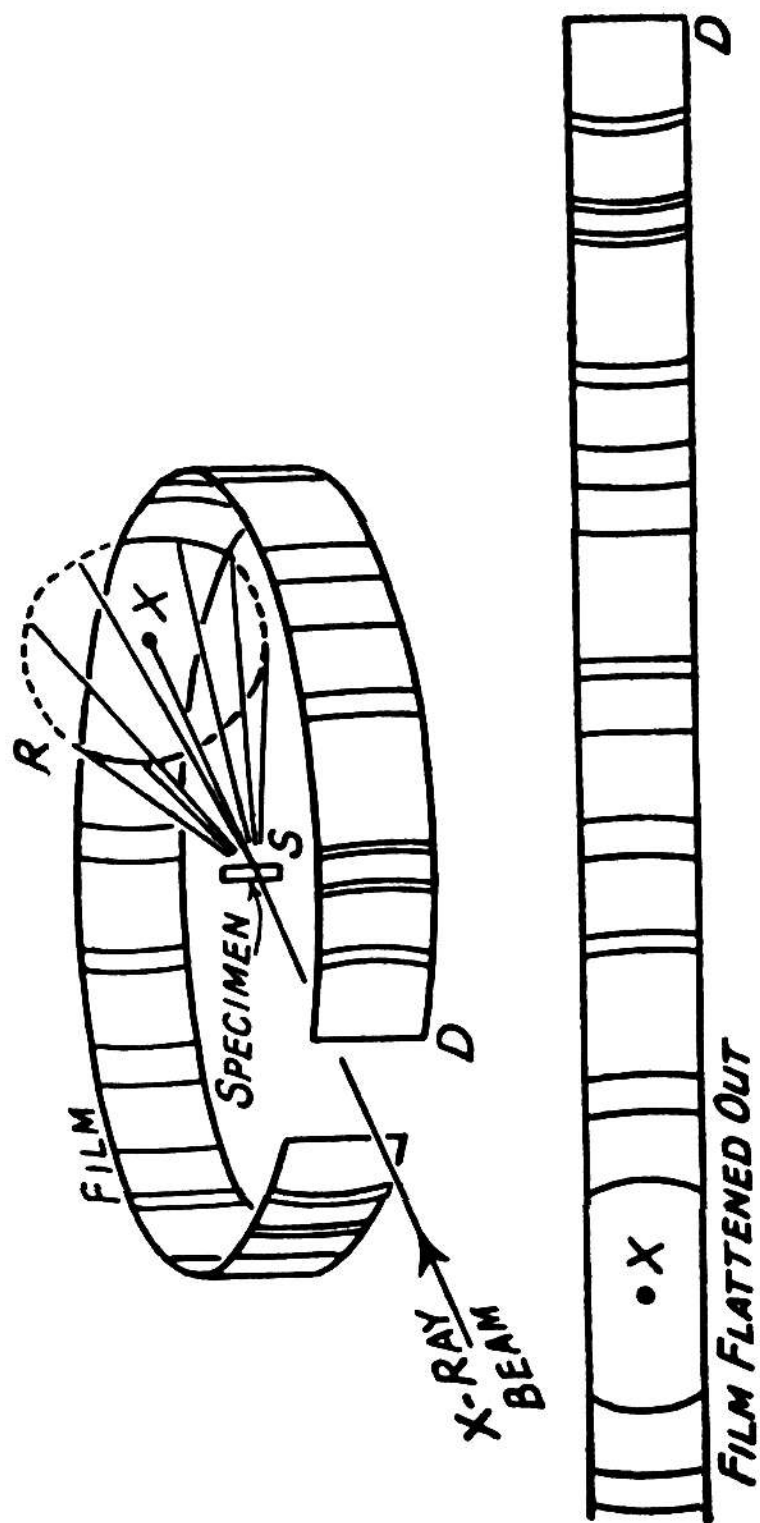


FIG. 1B Arrangement for taking powder photographs. The angle RSX is 2θ , where θ is the angle of incidence on a set of crystal planes.

three strongest lines being marked. Because of the difficulty inherent in analyzing a mixture such as concrete by powder x-ray techniques, it was not practical to apply this procedure in this study. This information is applied for future use with simple substances.

POWDER X-RAY DATA ON CEMENT MINERALS (15)

The values of I represent relative intensity.

The d values for the spacings are given in Å, Angstrom units, the intensities are on an arbitrary numerical scale, 10 being the strongest and 1 the weakest. Where it is known that doublets would be shown by using a camera of very high resolving power (such as the Guinier camera), the lines are marked with an asterisk. The three strongest lines are underlined. The symbol B indicates a broad line.

CaO [1]		MgO [1]		Ca(OH) ₂ [1]		Mg(OH) ₂ (Brucite) [1]	
d	I	d	I	d	I	d	I
<u>2.778</u>	8	2.431	1	<u>4.900</u>	7	<u>4.77</u>	8
<u>2.405</u>	10	2.106	10	3.112	2	2.725	2
<u>1.701</u>	9	<u>1.489</u>	9	2.628	10	2.365	10
1.451	6	1.270	1	2.447	1	<u>1.794</u>	7
1.390	3	<u>1.216</u>	2	1.927	4	1.573	6
1.203	1	1.0533	1	1.796	4	1.494	5
1.1036	1	0.9665	1	1.687	2	1.373	5
1.0755	4	0.9419	2	1.634	1	1.363	1
0.9819	4	0.8600	2	1.557	1	1.310	3
0.9258	1	0.8109	1	1.434	2	1.192	1
0.8504	1			1.449	2	1.183	2
0.8131	3			1.314	1	1.118	1
0.8018	3			1.228	1	1.092	1
				1.211	1	1.034	2
				1.762	1	1.030	1
				1.1432	2	1.0067	2
				1.1275	1		
				1.0599	2		
				1.0366	1		
				1.0143	2		

$3\text{CaO}.\text{SiO}_2[2]$		Alite [2]		$\alpha\ 2\text{CaO}.\text{SiO}_2[3]$		$\alpha'\ 2\text{CaO}.\text{SiO}_2[3]$	
d	I	d	I	d	I	d	I
5.901	4	3.861	3	4.69	2	4.74	2
3.862	3	3.517	1	3.87	2	4.63	1
3.510	2	3.334	2	3.41	2	3.82	2
3.346	2	3.144	2	3.15	2	3.40	2
3.227	1	3.022	8	3.02	1	3.14	2
3.022	8	2.959	6	2.88	7	2.89	2
2.957	6	2.880	2	2.83	2	2.81	2
2.891	3	2.804	1	2.76	9	2.76	10
2.818	1	2.764	10	2.71	10	2.75	10
2.776	10	2.739	9	2.54	2	2.69	8
2.730	8	2.682	3	2.46	1	2.63	2
2.670	1	2.592	9	2.35	2	2.36	2
2.602	10	2.436	3	2.305	2	2.28	2
2.549	1	2.313	6	2.208	7	2.23	2
2.449	3	2.178	9	2.129	1	2.200	6
2.326	6	2.172	6	2.072	2	2.137	1
2.304	5	2.089	1	2.052	2	2.082	1
2.277	2	2.060	1	2.008	1	2.035	6
2.234	1	2.208	1	1.971	2	1.965	2
2.185	10	1.973	5	1.935	7	1.939	6
2.159	1	1.928	6	1.870	1	1.914	1
2.125	3	1.831	5	1.837	1	1.786	1
2.083	4	1.819	5	1.806	2	1.755	2
2.045	2	1.799	2				
2.011	1	1.761	9				
1.979	6/B	1.689	2				
1.940	7	1.640	2				
1.926	6	1.623	8				
1.900	2/B	1.537	6				
1.863	1	1.522	2				
1.825	6/B	1.485	9				
1.797	3						
1.771	9(1)						
1.752	8(1)						
1.642	2						
1.632	8						
1.623	6						
1.543	6						
1.526	2						
1.513	2						
1.497	6						
1.481	6						

Pure $3\text{CaO}.\text{SiO}_2$ can be distinguished from Alite since at (1) it gives doublets instead of single lines.

β $2\text{CaO} \cdot \text{SiO}_2$ [5]		γ $2\text{CaO} \cdot \text{SiO}_2$ [4]		$3\text{CaO} \cdot \text{Al}_2\text{O}_3$ [5]	
d	I	d	I	d	I
4.920	1	5.625	4	4.08	2
4.645	1	4.320	4	3.34	1
3.790	3	4.047	2	2.70	10
3.380	1	3.794	4	2.39	2
3.335	1	3.354	2	2.258	1
3.090	1	3.002	10	2.200	5
3.040	2	2.881	2	1.984	1
2.874	2*	2.728	10	1.951	1
2.778	10*	2.525	2	1.907	9
2.740	10*	2.508	2	1.826	1
2.714	1	2.460	2	1.556	8
2.607	10	2.320	2	1.346	5
2.544	3	2.243	2	1.206	5
2.448	4*	2.186	2	1.106	2
2.403	4	2.024	2	1.023	5
2.279	3	1.963	2		
2.189	6*	1.928	8		
1.163	4	1.878	2		
2.128	1	1.800	6		
2.088	1*	1.751	6		
2.044	2	1.685	8		
2.019	1	1.669	2		
1.982	7	1.632	6		
1.911	1	1.539	2		
1.892	4	1.524	2		
1.844	1	1.498	2		
1.806	2	1.469	2		
1.787	2	1.457	2		
1.763	1	1.443	2		
1.706	3	1.414	2		
1.632	7	1.401	2		
1.606	4	1.374	2		
1.587	2	1.352	2		
1.573	2	1.268	2		
1.550	1 B				
1.523	4				
1.483	3				
1.448	1				
1.427	1				
1.416	1				
1.406	1				
1.393	1				

4CaO.Al ₂ O ₃ Fe ₂ O ₃ [5]		6CaO.2Al ₂ O ₃ [5]		2CaO.Fe ₂ O ₃ [5]	
d	I	d	I	d	I
7.24	5	7.17	5	7.36	4
3.63	3	4.87	2	5.23	1
3.39	1	3.62	4	3.88	2
2.77	8	3.37	1	3.68	4
2.67	7	2.99	1	3.05	2
2.63	10	2.76	8	2.78	7
2.57	2	2.69	1	2.71	6
2.43	1	2.65	8	2.67	10
2.20	3	2.62	10	2.60	2
2.15	3	2.56	4	2.35	1
2.04	6	2.44	1	2.22	1
1.92	8	2.41	1	2.18	3
1.86	2	2.19	6	2.07	5
1.81	4	2.14	6	1.94	7
1.73	2	2.04	7	1.90	1
1.57	4	1.91	8	1.88	2
1.53	4	1.85	3	1.84	4
1.51	1	1.81	6	1.74	3
1.50	2	1.79	1	1.66	1
1.45	1	1.72	4	1.62	2
1.42	1	1.66	1	1.59	4
1.39	2	1.60	2	1.55	4
1.33	1	1.57	6	1.54	1
1.32	2	1.56	1	1.52	2
		1.53	7	1.48	1
		1.51	2	1.46	1
		1.50	2	1.43	1
		1.45	2	1.38	1
		1.41	2	1.36	1
		1.38	3	1.34	4
		1.35	3		
		1.34	1		
		1.33	2		
		1.32	4		

Hillebrandite [9] (Synthetic) (C ₂ SH(B))		2CaO.Al ₂ O ₃ .8H ₂ O [5]		3CaO.Al ₂ O ₃ .6H ₂ O [5]	
d	I	d	I	d	I
12.0?	1	10.70	10	5.140	9
8.10	3	5.36	8	4.453	4
5.70	3	4.25	1	3.366	6
4.74	9	4.10	1	3.149	5
4.03	4	3.94	1	2.816	8
3.51	6	3.80	2	2.571	2
3.32	6	3.58	6	2.469	3
3.00	7	2.86	7	2.300	10
2.90	10	2.78	2	2.226	1
2.80	2	2.68	6	2.043	9
2.75	8	2.54	7	1.991	1
2.67	4	2.49	2	1.817	1
2.62	4	2.45	1	1.746	4
2.44	3	2.39	6	1.714	3
2.36	7	2.24	3	1.683	5
2.23	9	2.15	1	1.599	2
2.05	6	2.10	5	1.574	1
1.95	6	2.03	1	1.484	1
1.93	6	1.97	3	1.408	8
1.85	6	1.94	1	1.366	1
1.80	9	1.84	3	1.342	2
1.75	5	1.79	1		
1.71	2	1.73	1		
1.68	1	1.67	6		
1.66	1	1.65	4		
1.62	2	1.59	4		
1.56	2	1.51	2		
1.53	3	1.44	3		
1.52	2	1.42	1		
1.46	4	1.37	2		
1.44	2	1.09	3		
1.41	2	1.06	1		
1.35	1				
1.33	1				
1.32	2				
1.17	4				
1.11	2				
1.09	2				

$\text{CaO} \cdot \text{Al}_2\text{O}_3 \cdot 10\text{H}_2\text{O}$ [5]		$\text{CaO} \cdot \text{Al}_2\text{O}_3 \cdot 10\text{H}_2\text{O}$ [5]	
d	I	d	I
14.30	10	2.06	4
7.16	10	1.94	5
5.39	4	1.87	1
4.75	4	1.83	3
4.52	3	1.79	4
4.16	3	1.75	1
3.93	1	1.71	3
3.72	5	1.64	5
3.56	7	1.60	6
3.26	6	1.56	1
3.10	5	1.52	2
2.88	6	1.47	3
2.69	5	1.40	2
2.55	7	1.38	4
2.47	5	1.27	1
2.36	6	1.24	2
2.26	6	1.18	2
2.18	6	1.07	2
2.11	4		

CaO.Al ₂ O ₃ [7]		'Pleochroite' [8]		12CaO.7Al ₂ O ₃ [5]		CaO.2Al ₂ O ₃ [5]	
d	I	d	I	d	I	d	I
5.54	6	5.40	1	4.89	10	6.20	3
4.66	9	4.90	3	4.24	2	4.44	7
4.04	7	4.60	2	3.795	5	3.59	4
3.71	8	4.11	5	3.200	5	3.49	10
3.41	3	3.70	8	2.999	7	3.21	3
3.29	7	3.01	7	2.680	10	3.08	5
3.19	7	2.97	1	2.553	4	2.87	4
3.06	1 B	2.87	10	2.445	8	2.74	4
2.98		2.76	10	2.347	3	2.70	4
2.95	10	2.69	3	2.186	7	2.59	9
2.90	5	2.60	1	2.056	2	2.53	3
2.85	8	2.53	1	1.944	7	2.43	4
2.75	5	2.44	5	1.898	1	2.40	1
2.53		2.37	6	1.894	2	2.32	3
2.50	10	2.34	6	1.762	2	2.21	1
2.43	4	2.21	2	1.729	4	2.17	3
2.42		2.18	2	1.694	2	2.06	1
2.39	10	2.11	4	1.662	7	2.05	5
2.33	8	2.03	6	1.646	1	2.00	3
2.29	7	1.92	6	1.630	4	1.96	2
2.26	7	1.89	1	1.601	7	1.93	1
2.20		1.84	2	1.559	1	1.90	3
2.19	9	1.79	7	1.522	3	1.87	3
2.16	4	1.76	8	1.497	2	1.80	5
2.13	8	1.72	4	1.475	3	1.76	5
2.10	7	1.66	4	1.393	6	1.68	4
2.08	1 B	1.63	5	1.357	1	1.62	3
2.01	8	1.55	4	1.339	3	1.55	1
2.00	4	1.52	5	1.322	1	1.53	5
1.956	7	1.48	6	1.307	4	1.51	2
1.921	10	1.45	1	1.292	2	1.48	2
1.909	8	etc.		1.277	2	1.45	1
1.852	4			1.263	3	1.42	1
1.830	8			1.235	2	1.40	1
1.802	2			1.210	2	1.37	5
1.780	2			1.198	1	1.35	2
1.740	7			1.186	1	1.33	4
1.721	6			1.174	2	1.31	1
1.696	6					1.29	2
1.677	7					1.28	2
1.651	8					1.26	2
1.617	3					1.25	2
1.602	2					1.22	2

Calcium silicate hydrate (I) [9]		Calcium silicate hydrate (II) [9]		Afwillite [9]		2CaO.SiO ₂ α hydrate (C ₂ SH(A)) [9]	
d	I	d	I	d	I	d	I
9-14	10	9.80	9	6.45	8	5.35	3
3.06	10	4.90	2	5.74	8	4.63	1
2.81	8	3.07	10	5.08	5	4.22	9
1.83	8	2.85	5	4.73	8	3.90	8
1.67	4	2.80	9	4.15	5	3.54	8
1.53	2	2.40	4	3.91	5	3.27	10
1.40	4	2.20	1	3.75	5	2.04	3
1.17	1	2.10	1	3.28	5	2.87	8
1.11	2	2.00	6	3.19	10	2.80	8
1.07	1	1.83	9	3.05	5	2.77	3
This is the data for the poorly crystalline material. The long spacing can vary con- siderably and may also be undetected.		1.72	1	2.84	10	2.71	3
		1.62	1	2.74	10	2.69	2
		1.56	5	2.67	5	2.65	6
		1.40	4	2.59	5	2.60	8
		1.225	3	2.44	4	2.56	3
		1.165	3	2.35	6	2.52	6
		1.100	1	2.31	5	2.47	1
		1.045	2	2.21	5	2.41	9
		1.025	1	1.145	8	2.31	2
		1.000	1	2.064	4	2.27	2
				2.017	4	2.24	3
				1.989	6	2.18	5
				1.949	8	2.16	3
				1.924	5	2.10	2
				1.862	6	2.08	3
				1.805	8	2.06	4
				1.776	8	2.03	3
				1.724	4	2.02	3
				1.704	6	1.982	5
				1.683	6	1.956	3
				1.630	6	1.926	5
				1.604	8	1.890	3
				1.589	6	1.872	4
				1.563	4	1.842	2
				1.507	5	1.820	5
				1.413	4	1.788	8
				1.382	4	1.737	4
				1.380	4	1.712	4
				1.309	4	1.687	1
				1.345	4	1.662	4
				1.265	4	1.654	5

$4\text{CaO} \cdot \text{Al}_2\text{O}_3 \cdot 13\text{H}_2\text{O}$ [5]		Ettringite $3\text{CaO} \cdot \text{Al}_2\text{O}_3 \cdot 3\text{CaSO}_4 \cdot 32\text{H}_2\text{O}$ [5]		$3\text{CaO} \cdot \text{Al}_2\text{O}_3 \cdot \text{CaSO}_4 \cdot 13\text{H}_2\text{O}$ [5]	
d	I	d	I	d	I
8.05	10	9.80	10	8.92	10
4.50	1	5.70	8	4.88	1
4.05	2	4.90	6	4.72	1
3.90	5	4.67	7	4.46	6
3.63	1	4.34	2	3.99	6
2.86	9	3.87	8	3.65	1
2.69	6	3.60	3	2.87	7
2.54	3	3.45	6	2.73	4
2.45	6	3.26	4	2.60	1
2.36	3	3.02	3	2.45	6
2.23	4	2.79	9	2.41	5
2.17	1	2.67	3	2.35	1
2.04	2	2.57	8	2.33	2
1.97	3	2.43	3	2.25	2
1.93	2	2.36	1	2.19	2
1.86	3	2.20	8	2.06	4
1.74	2	2.14	6	1.99	2
1.66	8	2.06	3	1.90	1
		1.94	3	1.87	1
		1.89	2	1.82	4
		1.84	4	1.66	5
		1.80	1	1.63	4
		1.75	4	1.58	1
		1.70	4	1.55	1
		1.66	6	1.54	1
		1.62	2	1.44	2
		1.57	4	1.42	1
		1.54	2	1.39	2
		1.50	4	1.37	1
		1.45	3	1.35	1
		1.34	3		
		1.30	3		

APPENDIX C

Data for the thermal Decomposition of the Powdered Carbonate

Table 1-C. CO_2 Production Rate with Time for
Unirradiated CaCO_3 at 1621°F

CO_2 Production Rate (ml/min.g dried carbonate)					
Time (min)	Run No. 1	Run No. 2	Run No. 3	Run No. 4	Average
2	-----	0.158	0.036	0.081	0.069 ± 0.068
4	0.133	0.216	0.141	0.199	0.172 ± 0.041
6	0.156	0.238	0.139	0.206	0.185 ± 0.046
8	0.162	0.219	0.134	0.1213	0.182 ± 0.041
10	0.150	0.218	0.131	0.193	0.173 ± 0.040
12	0.146	0.207	0.135	0.195	0.171 ± 0.035
14	0.143	0.187	0.123	0.185	0.160 ± 0.032
16	0.139	0.176	0.116	0.172	0.151 ± 0.021
18	0.136	0.165	0.111	0.155	0.142 ± 0.024
20	0.134	0.146	0.105	0.154	0.135 ± 0.022
22	0.120	0.128	0.107	0.136	0.123 ± 0.012
24	0.117	0.101	0.089	0.108	0.104 ± 0.012
26	0.114	0.064	0.094	0.082	0.086 ± 0.021
28	0.098	0.047	0.088	0.062	0.073 ± 0.019
30	0.102	0.030	0.086	0.044	0.066 ± 0.034
32	0.092	0.008	0.084	0.026	0.055 ± 0.042
34	0.082		0.074	0.015	0.043 ± 0.041
36	0.073		0.068	0.003	0.036 ± 0.040
38	0.064		0.065		0.032 ± 0.037
40	0.057		0.054		0.028 ± 0.032
42	0.048		0.049		0.024 ± 0.028
44	0.045		0.049		0.024 ± 0.027
46	0.034		0.036		0.018 ± 0.020
48	0.032		0.033		0.016 ± 0.016
50	0.031		0.025		0.014 ± 0.014
52	0.035		0.019		0.014 ± 0.017
54	0.035		0.016		0.013 ± 0.017
56	0.015		0.003		0.005 ± 0.007
58	0.006		0.002		0.002 ± 0.003
60	0.002		-----		0.005 ± 0.001
Total CO_2 (ml/g dried sample)	5.002	4.616	4.424	4.454	4.624 ± 0.281
W_s (g)	1.7122	1.5824	1.7263	1.6206	1.6604 ± 0.07
W_l (g)	0.7426	0.6822	0.6994	0.7069	0.7078 ± 0.0514
W_l (g)/ W_s (g)	0.4262	0.4311	0.4051	0.4362	0.4247 ± 0.0137

Table 2-C CO_2 Production Rate with Time for
Irradiated CaCO_3 at 1621°F

CO_2 Production Rate (ml/min.g dried carbonate)				
Time (min)	31.2 Mrad*			Average
	Run No. 1	Run No. 2	Run No. 3	
2	0.052	-----	-----	0.017 ± 0.030
4	0.192	0.130	0.195	0.172 ± 0.037
6	0.195	0.156	0.193	0.181 ± 0.022
8	0.205	0.158	0.188	0.184 ± 0.024
10	0.195	0.151	0.188	0.178 ± 0.024
12	0.225	0.158	0.184	0.189 ± 0.034
14	0.178	0.149	0.169	0.165 ± 0.015
16	0.175	0.146	0.157	0.159 ± 0.015
18	0.165	0.148	0.150	0.154 ± 0.009
20	0.155	0.144	0.147	0.149 ± 0.006
22	0.158	0.130	0.123	0.137 ± 0.019
24	0.145	0.135	0.116	0.132 ± 0.015
26	0.135	0.130	0.104	0.123 ± 0.017
28	0.123	0.133	0.087	0.114 ± 0.024
30	0.090	0.128	0.077	0.098 ± 0.027
32	0.097	0.116	0.056	0.090 ± 0.031
34	0.077	0.112	0.043	0.077 ± 0.035
36	0.067	0.099	0.033	0.066 ± 0.033
38	0.060	0.096	0.024	0.060 ± 0.036
40	0.045	0.087	0.012	0.048 ± 0.038
42	0.033	0.085	0.007	0.042 ± 0.040
44	0.027	0.083		0.037 ± 0.042
46	0.023	0.069		0.031 ± 0.035
48	0.009	0.067		0.025 ± 0.036
50	0.005	0.057		0.021 ± 0.032
52		0.053		0.018 ± 0.031
54		0.051		0.017 ± 0.030
56		0.041		0.014 ± 0.024
58		0.043		0.014 ± 0.024
60		0.034		0.011 ± 0.020
Total CO_2 (ml/g dried sample)	5.662	6.348	4.506	5.5050 ± 0.242
W_s (g)	1.5005	1.6492	1.4526	1.5341 ± 0.1025
W_1 (g)	0.6159	0.5264	0.5990	0.5804 ± 0.0474
W_1 (g) / W_s (g)	0.4105	0.3192	0.4124	0.3807 ± 0.0534

*Co-60 Gamma-Ray Irradiation

Table 3-C CO_2 Production Rate with Time for
Irradiated CaCO_3 at 1621°F

CO_2 Production Rate (ml/min.g dried carbonate)			
Time (min)	21.2 Mrad*		Average
	Run No. 1	Run No. 2	
2	0.127	0.074	0.101 ± 0.038
4	0.142	0.173	0.158 ± 0.022
6	0.150	0.178	0.164 ± 0.020
8	0.144	0.176	0.160 ± 0.023
10	0.141	0.166	0.154 ± 0.018
12	0.138	0.159	0.149 ± 0.015
14	0.125	0.156	0.141 ± 0.022
16	0.121	0.145	0.133 ± 0.017
18	0.112	0.133	0.124 ± 0.015
20	0.114	0.121	0.118 ± 0.005
22	0.097	0.116	0.107 ± 0.014
24	0.093	0.099	0.096 ± 0.004
26	0.087	0.090	0.089 ± 0.002
28	0.075	0.069	0.072 ± 0.004
30	0.073	0.057	0.065 ± 0.011
32	0.060	0.047	0.054 ± 0.009
34	0.052	0.033	0.043 ± 0.009
36	0.046	0.021	0.034 ± 0.018
38	0.046	0.010	0.028 ± 0.026
40	0.033	0.007	0.020 ± 0.018
42	0.022		0.011 ± 0.016
44	0.015		0.008 ± 0.011
46	0.011		0.006 ± 0.008
48	0.011		0.006 ± 0.008
50	0.003		0.002 ± 0.002
Total CO_2 (ml/g dried sample)	4.076	4.060	4.068 ± 0.08232
W_s (g)	1.6727	1.4454	1.5591 ± 0.1608
W_1 (g)	0.6850	0.5372	0.6111 ± 0.1045
W_1 (g)/ W_s (g)	0.4095	0.3719	0.3906 ± 0.0267

*Co-60 Gamma-Ray Irradiation

Table 4-C CO_2 Production Rate with Time for
Irradiated CaCO_3 at 1621°F

CO_2 Production Rate (ml/min.g dried carbonate)			
Time (min)	16.03 Mrad*		Average
	Run No. 1	Run No. 2	
2	0.121	0.057	0.089 ± 0.045
4	0.154	0.152	0.153 ± 0.001
6	0.170	0.158	0.164 ± 0.009
8	0.167	0.155	0.161 ± 0.009
10	0.162	0.149	0.156 ± 0.009
12	0.152	0.133	0.143 ± 0.014
14	0.151	0.131	0.141 ± 0.014
16	0.134	0.128	0.131 ± 0.004
18	0.136	0.120	0.128 ± 0.011
20	0.121	0.107	0.114 ± 0.010
22	0.098	0.095	0.097 ± 0.002
24	0.074	0.082	0.078 ± 0.006
26	0.062	0.066	0.064 ± 0.003
28	0.033	0.046	0.040 ± 0.010
30	0.021	0.036	0.029 ± 0.011
32		0.019	0.010 ± 0.014
34		0.006	0.003 ± 0.004
<hr/>			
Total CO_2 (ml/g dried sample)	3.512	3.280	3.402 ± 0.058
<hr/>			
W_s (g)	1.5282	1.5825	1.5554 ± 0.0384
<hr/>			
W_l (g)	0.6612	0.6519	0.6566 ± 0.0066
<hr/>			
W_l (g)/ W_s (g)	0.4327	0.4119	0.4223 ± 0.0147

*Co-60 Gamma-Ray Irradiation

Data for the Thermal Decomposition of the Powdered
Kapitzke Concrete

Table 5-C CO₂ Production Rate with Time for
Unirradiated Concrete at 1621°F

CO ₂ Production Rate (ml/min.g dried concrete)					
Time (min)	Run No. 1	Run No. 2	Run No. 3	Run No. 4	Average
2	0.474	0.398	0.244	0.189	0.326 ± 0.132
4	0.242	0.239	0.314	0.383	0.295 ± 0.068
6	0.137	0.172	0.176	0.168	0.163 ± 0.018
8	0.132	0.165	0.155	0.125	0.144 ± 0.019
10	0.134	0.160	0.147	0.136	0.144 ± 0.014
12	0.113	0.168	0.145	0.134	0.140 ± 0.023
14	0.123	0.144	0.131	0.124	0.131 ± 0.009
16	0.115	0.140	0.131	0.120	0.128 ± 0.012
18	0.112	0.133	0.131	0.124	0.126 ± 0.012
20	0.103	0.122	0.116	0.120	0.115 ± 0.009
22	0.098	0.114	0.114	0.112	0.110 ± 0.008
24	0.091	0.104	0.108	0.098	0.100 ± 0.007
26	0.080	0.091	0.097	0.084	0.088 ± 0.008
28	0.073	0.079	0.088	0.075	0.079 ± 0.007
30	0.066	0.062	0.075	0.066	0.067 ± 0.006
32	0.052	0.052	0.070	0.058	0.058 ± 0.009
34	0.047	0.043	0.059	0.048	0.049 ± 0.007
36	0.042	0.038	0.054	0.043	0.044 ± 0.007
38	0.031	0.026	0.048	0.034	0.035 ± 0.009
40	0.031	0.018	0.044	0.027	0.030 ± 0.011
42	0.023	0.013	0.033	0.020	0.022 ± 0.008
44	0.013	0.007	0.029	0.018	0.017 ± 0.009
46	0.007	0.005	0.025	0.014	0.013 ± 0.009
48	0.010	0.003	0.019	0.010	0.011 ± 0.007
50	0.002		0.012	0.004	0.005 ± 0.005
52			0.0097	0.0032	0.003 ± 0.005
54			0.006		0.002 ± 0.003
56			0.0048		0.001 ± 0.002
58			0.0024		0.001 ± 0.001
Total CO ₂ (ml/g dried sample)	4.700	4.992	5.196	4.7064	4.899 ± 0.158
W _s (g)	2.1293	2.5688	2.0698	2.3480	2.2790 ± 0.2273
W ₁ (g)	0.3221	0.4073	0.3195	0.3880	0.3592 ± 0.0673
W ₁ (g)/W _s (g)	0.1513	0.1586	0.1544	0.1653	0.1574 ± 0.0061

Table 6-C CO₂ Production Rate with Time for
Irradiated Concrete at 1621°F

CO ₂ Production Rate (ml/min.g dried concrete)			
Time (min)	24.7 Mrad* & 11.11×10^{18} n/cm ²		
	Run No. 1	Run No. 2	Average
2	0.322	0.290	0.306 ± 0.036
4	0.098	0.124	0.111 ± 0.018
6	0.148	0.083	0.116 ± 0.033
8	0.103	0.076	0.090 ± 0.042
10	0.088	0.084	0.086 ± 0.003
12	0.096	0.077	0.087 ± 0.014
14	0.091	0.069	0.080 ± 0.016
16	0.087	0.068	0.078 ± 0.014
18	0.077	0.058	0.068 ± 0.014
20	0.074	0.054	0.064 ± 0.014
22	0.063	0.048	0.056 ± 0.011
24	0.050	0.043	0.047 ± 0.005
26	0.034	0.035	0.035 ± 0.001
28	0.033	0.024	0.029 ± 0.005
30	0.027	0.021	0.024 ± 0.004
32	0.016	0.010	0.013 ± 0.004
34	0.004	0.006	0.005 ± 0.0014
36	0.001		0.0005 ± 0.0007
Total CO ₂ (ml/g dried sample)	2.824	2.341	2.583 ± 0.057
W _s (g)	1.8885	0.8098	1.8492 ± 0.0557
W ₁ (g)	0.3164	0.3005	0.3085 ± 0.01124
W ₁ (g)/W _s (g)	0.1675	0.1660	0.1668 ± 0.0011

*Co-60 Gamma-Ray Irradiation

Table 7-C CO₂ Production Rate with Time for
Irradiated Concrete at 1621°F

CO ₂ Production Rate (ml/min.g dried concrete)	
Time (min)	12.2 Mrad* & 54.95×10^{16} n/cm ²
2	0.166
4	0.054
6	0.062
8	0.067
10	0.052
12	0.048
14	0.038
16	0.035
18	0.023
20	0.008
Total CO ₂ (ml/g dried sample)	1.106
W _s (g)	1.8693
W ₁ (g)	0.3478
W ₁ (g)/W _s (g)	0.1861

*Co-60 Gamma-Ray Irradiation

Table 8-C CO₂ Production Rate with Time for
Irradiated Concrete at 1621°F

CO ₂ Production Rate (ml/min.g dried concrete)				
Time (min)	19.9332 Mrad*			Average
	Run No. 1	Run No. 2	Run No. 3	
2	0.134	0.120	0.162	0.130 \pm 0.021
4	0.069	0.091	0.054	0.071 \pm 0.019
6	0.072	0.083	0.063	0.073 \pm 0.007
8	0.073	0.071	0.061	0.068 \pm 0.006
10	0.065	0.060	0.054	0.060 \pm 0.008
12	0.043	0.045	0.051	0.046 \pm 0.004
14	0.026	0.031	0.049	0.035 \pm 0.012
16	0.010	0.007	0.040	0.019 \pm 0.018
18			0.033	0.011 \pm 0.019
20			0.027	0.009 \pm 0.016
22			0.017	0.006 \pm 0.010
24			0.004	0.001 \pm 0.002
Total CO ₂ (ml/g dried sample)	0.984	1.016	1.230	1.077 \pm 0.046
W _s (g)	2.332	2.2006	2.2652	2.1663 \pm 0.0751
W _l (g)	0.3615	0.3994	0.3634	0.3748 \pm 0.0214
W _l (g)/W _s (g)	0.1778	0.1815	0.1604	0.1732 \pm 0.0108

*Co-60 Gamma-Ray Irradiation

Table 9-C Values of α calculated by two methods for CaCO_3 .

Gas Chromatographic Method		Weighing Method			
t	α	t	W_o (g)	W_i (g)	α
2	0.00302	0	1.5435		
4	0.00149	2		1.5318	0.018
6	0.00266	5		1.5268	0.025
8	0.00379	10		1.5214	0.032
10	0.00489	15		1.5143	0.043
12	0.00602	20		1.5103	0.048
14	0.00705	25		1.5053	0.057
16	0.00804	30		1.4976	0.068
18	0.00897	35		1.4908	0.077
20	0.00985	45		1.4778	0.098
22	0.01075	50		1.4726	0.105
24	0.01550	60		1.4628	0.118
26	0.01229				
28	0.01303				
30	0.01375				
32	0.01446				
34	0.01508				
36	0.01565				
38	0.01620				
40	0.016654				
42	0.017071				
44	0.017483				
46	0.017785				
48	0.018062				
50	0.018272				
52	0.018432				
54	0.018566				
56	0.0185912				
58	0.018608				

Table 10-C Values of α calculated by two methods for Kapitzke concrete.

t	α	t	W_o (g)	W_i (g)	α
2	0.0095	0	2.2836		
4	0.02175	2		2.214	0.125
6	0.02861	5		2.1946	0.181
8	0.03466	10		2.1668	0.236
10	0.04039	15		2.1557	0.259
12	0.04605	20		2.1410	0.292
14	0.05116	25		2.1371	0.296
16	0.05627	35		2.1232	0.324
18	0.06138	45		2.1203	0.333
20	0.06590	60		2.1070	0.361
22	0.07035				
24	0.07456				
26	0.07834				
28	0.08177				
30	0.08470				
32	0.08743				
34	0.08973				
36	0.09184				
38	0.09371				
40	0.09543				
42	0.09672				
44	0.09785				
46	0.09883				
48	0.09957				
50	0.10004				
52	0.10042				
54	0.10065				
56	0.10084				
58	0.10093				

Table 11-C CO₂ Production Rate with Time for
Irradiated Concrete at 1621°F

CO ₂ Production Rate (ml/min·g dried concrete)		
Time (min)	12.2 Mrad*	24.7 Mrad*
2	0.0910	0.0786
4	0.0745	0.0632
6	0.0514	0.0446
8	0.0461	0.0473
10	0.0488	0.0486
12	0.0488	0.0486
14	0.0508	0.0466
16	0.0488	0.0479
18	0.0514	0.0459
20	0.0461	0.0439
22	0.0448	0.0386
24	0.0428	0.0340
26	0.0402	0.0333
28	0.0342	0.0273
30	0.0298	0.0226
32	0.0257	0.0180
34	0.0231	0.0153
36	0.0172	0.0140
38	0.0132	0.0998
40	0.0099	0.0092
42	0.0073	0.0072
44	0.0059	0.0053
46	0.0064	0.0040
48	0.0040	0.0027
50	0.0026	0.0013
52	0.0013	
<hr/>		
Total CO ₂ (ml/g dried sample)	1.7365	1.5182
<hr/>		
W _s (g)	2.4268	2.4037
<hr/>		
W ₁ (g)	0.4199	0.4616
<hr/>		
W ₁ (g)/W _s (g)	0.1731	0.1920
<hr/>		

* Co-60 Gamma-Ray Irradiation

Appendix D

"Meyer Concrete" (1)

Kapitzke concrete constituents are reported to be as follows:

Table 1-D Constituents of Kapitzke Concrete in
Atomic Density Units.

Constituents	Atomic Density (atoms/cm ³)
Ca	7.35×10^{21}
H	10.4×10^{21}
O	45.1×10^{21}
C	5.0×10^{21}

Specific gravity and water content of Kapitzke concrete were respectively 2.4 and 6.4%.

Kapitzke concrete is similar to "Meyer Concrete". Meyer Concrete constituents are described below

Table 2-D Chemical Analysis of "Meyer Concrete."

Constituents	R ₍₁₉₎ Wet Analysis, Weight %	R ₍₂₀₎ Wet Analysis, Weight %	R ₍₁₉₎ X-Ray Emission Weight %
Total Silica	38.78	44.09	38.10
Soluble Silica	3.06		
Ferric Oxide	2.34	1.75	2.01
Aluminum Oxide	3.29	0.25	3.52
Calcium Oxide	31.10	30.55	30.00
Magnesium Oxide	1.33	0.90	
Sulfur Trioxide	0.21	0.26	
Loss on Ignition	21.68	21.61	
Insoluble Residue	40.76	41.06	
Sodium Oxide	0.00	0.25	
Potassium Oxide	0.08	0.33	0.89
Titanium Dioxide		not determined	0.25
Carbon Dioxide		13.24	
Combined Water		8.37	
loss--CO ₂			
Total		99.99	

Where $R_{(19)}$ = Reference 19

$R_{(20)}$ = Reference 20

Note: Reference 20 states, the sample as received appeared to be slightly wet. Therefore the entire sample was oven dried (120°C) over night prior to any analysis. Free water was 0.53%.

RADIATION EFFECTS ON CONCRETE

by

Hamza K. Al-Dujaili

B.Sc., The University of Baghdad, 1962

AN ABSTRACT OF A MASTER'S THESIS

submitted in partial fulfillment of the
requirements for the degree

MASTER OF SCIENCE

Department of Nuclear Engineering

KANSAS STATE UNIVERSITY

Manhattan, Kansas

1972

ABSTRACT

Powdered calcium carbonate was isothermally decomposed to CaO and carbon dioxide gas in an inert atmosphere of flowing helium at a temperature of 1621°F. Samples of powdered concrete were similarly decomposed. The thermal decomposition of both materials was followed by periodically measuring the carbon dioxide content of the helium flow with a gas chromatography system. Chromatographic output measurements were used to calculate the carbon dioxide production rate as a function of time for each of the decompositions.

In comparison with unirradiated samples thermal decomposition at 1621°F of both powdered concrete and calcium carbonate irradiated with Co-60 gamma-rays exhibited an initial decrease in carbon dioxide production rates followed by an increasing rate with increasing dose. Histograms and tables of carbon dioxide production rates as a function of time are included. Irradiation with neutrons in addition to gamma rays at lower neutron fluences produced a further decrease in CO₂ production rate as compared with the same gamma-ray dose in the absence of the neutron fluence. An increase in neutron fluence at higher gamma-ray doses brought about a further increase in CO₂ production rate over that noted for samples irradiated with the gamma-rays only.

The decomposition of the powdered calcium carbonate and concrete were both found to follow an apparent surface controlled process. Both the powdered calcium carbonate and concrete showed no diffusion limiting phenomenon during the decomposition period.

A mixture of powdered Kapitzke concrete and aluminum metal with water in a plastic bottle were found to exhibit a vigorous chemical reaction releasing hydrogen gas. Mixtures containing powdered zinc or iron metal in

place of the aluminum, showed respectively a slow and no detectable chemical reaction. It appears that gas explosions of aluminum canned concrete shielding plugs reported in the literature are due to a chemical reaction between aluminum, concrete and water rather than a radiation induced decomposition of the concrete. Radiation, however, may release the combined water necessary to initiate the concrete-aluminum reaction.